

POLITECNICO DI TORINO

Corso di Laurea Magistrale
in Ingegneria Energetica e Nucleare

Preparation and Testing of Ceria-Based Catalyst for Hydrogen Production



Tesi di Laurea Magistrale

Relatori:

Prof. Massimo Santarelli

Dott. Domenico Ferrero

Dott. Paolo Marocco

Dott. Azharuddin

Candidato:

Marco Furini

2018

Abstract

The thesis work focused in the synthesis and the subsequent test of a novel Ceria-based oxides for the water splitting in a thermochemical looping, which is based on the cyclic reduction and re-oxidation of the metal oxides.

The samples were synthesized with the collaboration of the *Università degli studi di Udine* in Udine and they are characterized by a different Ceria-Zirconia and Ceria-Zirconia-Tin content.

The synthesis was performed using a specific sol-gel technique, the Pechini Method.

The experimental section were performed using a fixed-bed configuration in a micro-reactor and tests were carried out always at ambient pressure while testing different sample in order to understand which perform better.

List of contents:

| | |
|--|----|
| 1 INTRODUCTION | 1 |
| 1.1 The necessity to store solar energy | 1 |
| 1.2 Solar utilities | 3 |
| 1.2.1 Technologies | 3 |
| 1.2.2 Reactors | 5 |
| 1.3 Thermochemical splitting of the water | 6 |
| 1.3.1 Two-step thermochemical cycles | 7 |
| 2 SYNTHESIS AND CHARACTERIZATION | 11 |
| 2.1 The Sol-Gel Techniques | 11 |
| 2.2 Calculations for the synthesis of catalyst | 14 |
| 2.2.1 Synthesis of Ceria Zirconia oxide doped with Tin | 14 |
| 2.2.2 Summary of the results | 17 |
| 2.3 Characterization of the Catalyst | 18 |
| 2.3.1 Simultaneous Thermal Analysis | 18 |
| 2.3.2 SDT Results | 20 |
| 2.3.3 Brunauer-Emmett-Teller | 21 |
| 2.3.4 X-Ray powder diffraction | 23 |
| 3 EXPERIMENTAL | 27 |
| 3.1 Water splitting reaction tests setup | 27 |
| 3.2 The furnace-reactor system | 30 |
| 3.3 TCD gas analyser | 32 |
| 3.3.1 Measuring Principles | 32 |
| 3.4 Mass Spectrometer | 36 |
| 3.3.1 Ion source | 38 |

| | |
|--|-----------|
| 3.4.2 Mass analyser | 39 |
| 3.4.3 Ion detectors..... | 40 |
| 3.5 Experimental procedure..... | 44 |
| 3.6 Data Elaboration | 46 |
| 4 RESULTS | 49 |
| 4.1 Summary of the experiments..... | 49 |
| 4.2 CZ80 HSA: WS experiments with hydrogen reduction | 51 |
| 4.2.1 WS results (TCD measure) | 52 |
| 4.2.2 Water Splitting results (MS)..... | 54 |
| 4.4 CZ80 HSA: WS with thermal reduction | 58 |
| 4.4.1 The experimental procedure | 58 |
| 4.4.2 Results..... | 59 |
| 4.5 WS on the CZ80 – 0.15SnO₂ with thermal reduction | 61 |
| 4.6 WS on CZ20 – 0.25SnO₂ with thermal reduction..... | 63 |
| 4.7 WS on CZ80 – 0.15SnO₂ with hydrogen reduction | 63 |
| 4.8 WS on CZ20 with hydrogen reduction | 65 |
| 4.8 WS on CZ50 with hydrogen reduction | 66 |
| 4.9 WS on CZ80 with hydrogen reduction | 67 |
| 5 CONCLUSION | 69 |
| 6 BIBLIOGRAPHY..... | 71 |

List of figures

| | |
|--|----|
| Figure 1.1 Schematic of a solar refinery and solar fuel feedstock [4] | 2 |
| Figure 1.2 Schematic of a horizontal on-axis solar furnace [5] | 3 |
| Figure 1.3 Schematic of a vertical on-axis solar furnace [5] | 3 |
| Figure 1.4 Schematic of an off-axis solar furnace [6] | 4 |
| Figure 1.5 A beam down solar facility [6]. | 5 |
| Figure 1.6 Variation of Gibbs free energy, Enthalpy and Entropy with respect to the Temperature [7]. | 6 |
| Figure 1.7 Scheme of the two-step thermochemical reaction. | 7 |
| Figure 2.1 Solution of Ceria precursor in citric acid and water; The clearness of the solution indicates no metal precipitation. | 12 |
| Figure 2.2 The gel after the polyesterification. | 13 |
| Figure 2.3 Before after the first calcination treatment. | 13 |
| Figure 2.4 The SDT Q600 in the Udine Chemical Department during working operation. | 19 |
| Figure 2.5 Particular of the preliminary operation for the STA session. | 19 |
| Figure 2.6 Reduction extent of the 15% weight Tin doped sample. | 20 |
| Figure 2.7 Reduction extent of the 25% weight Tin doped sample. | 20 |
| Figure 2.8 Set-up procedure: heat under vacuum to erase organic trace. | 21 |
| Figure 2.9 Setup procedure, preparation and measuring. | 23 |
| Figure 2.10 Working principle scheme of XRD. | 23 |
| Figure 2.11 CZ 80 XRD crystal phase. | 24 |
| Figure 2.12 CZ 20 XRD crystal phase. | 24 |
| Figure 2.13 Tin oxide XRD crystal phase. | 25 |
| Figure 2.14 CZ80-0.15SnO ₂ XRD crystal phase. | 25 |
| Figure 2.15 CZ20-0.25SnO ₂ XRD crystal phase. | 26 |
| Figure 3.1 Scheme of the set-up. | 28 |
| Figure 3.2 Pictograms legend. | 29 |
| Figure 3.3 Top view of the alumina bar | 30 |
| Figure 3.4 Cross section of the alumina bar | 30 |
| Figure 3.5 The furnace device, on the left side of the picture are shown the alumina cylinders that holds the reactor bar in the work tube. | 31 |

| | |
|---|----|
| Figure 3.6 Scheme of a Thermal Conductivity Detector..... | 32 |
| Figure 3.7 NDIR detector scheme..... | 35 |
| Figure 3.8 Front view of the X-STREAM gas analyser. | 35 |
| Figure 3.9 The working principle of the mass spectrometer | 36 |
| Figure 3.10 Scheme of EII source scheme [20]. | 38 |
| Figure 3.11 Scheme of Faraday Cup [21]. | 40 |
| Figure 3.12 Scheme of discrete-dynode SEM, the blue arrows represent the multiplying effect that increase the ion current [22]. | 41 |
| Figure 3.13 Scheme of continuous-dynode SEM, the blue arrows represent the multiplying effect that increase the ion current [22]. | 42 |
| Figure 3.14 Mass Spectrometer assembly..... | 43 |
| Figure 3.15 Hydrogen partial pressure measured by MS | 46 |
| Figure 3.16 Purge-Peak pair..... | 47 |
| Figure 4.1 Visual look to the sample..... | 51 |
| Figure 4.2 Overall shape of ten consecutive cycle..... | 52 |
| Figure 4.3 Typical trend of hydrogen production | 53 |
| Figure 4.4 Hydrogen production comparison with and without thermal treatment..... | 54 |
| Figure 4.5 Different hydrogen production between thermal treatment. | 54 |
| Figure 4.6 Peak rate comparison. | 55 |
| Figure 4.7 Shape of the peak during the oxidation reaction | 56 |
| Figure 4.8 Hydrogen yield for each cycle..... | 57 |
| Figure 4.9 Peak rate for each cycle | 57 |
| Figure 4.10 Hydrogen yield for each cycle..... | 60 |
| Figure 4.11 Peak for each cycle..... | 60 |
| Figure 4.12 Hydrogen yield for each cycle..... | 62 |
| Figure 4.13 Peak rate for each cycle | 62 |
| Figure 4.14 Hydrogen yield for each cycle..... | 64 |
| Figure 4.15 Peak rate for each cycle | 64 |
| Figure 4.16 Hydrogen yield for each cycle..... | 65 |
| Figure 4.17 Peak rate for each cycle | 66 |
| Figure 4.18 Hydrogen yield for each cycle..... | 67 |
| Figure 4.19 Peak rate for each cycle | 68 |

1 INTRODUCTION

1.1 *The necessity to store solar energy*

One of the most discussed problem in the contemporary age is the climate change caused by global warming. Almost the whole scientific researches agree with the fact that those changing are caused by anthropic activity and, sadly, those changing are more and more affecting the human living and the stress towards the environment. The most responsible of such phenomenon are the greenhouse gases, which the most dangerous, in the long term, is the carbon dioxide. The actual efforts to lead towards a cleaner way to produce energy with renewable sources and thus reducing CO₂ production are not enough to guarantee a good scenario in the near future [1]. In order to keep CO₂ below a certain threshold or, even better, reverse the trend of carbon dioxide grow with the increasing of the global energy demand, different solutions can be adopted. There are two possible pathways to follow, one is the carbon capture and sequestration, the other one is the direct conversion of exhausted CO₂ in energy carrier. The idea behind the former technology is to store underground but, despite promising, CCS technologies have some not negligible drawbacks, among which, the need of lot of space, or if absent, the energy to make it.

The direct conversion of CO₂ in fuel through renewable source is an alternative way to store energy in a sun-to-fuel process aimed to the GHG neutralization.

Moreover, a true energy conversion can't leave out the transition to clean fuel on the in-wheel sector; thanks to their ready availability, high energy density and ease of handling, storage, fossil fuels supply the overall energy needs, and, even more, they supply energy in the transportation sector.

Indeed, the combustion of these fuels in order to extract their chemical energy is the main source of greenhouse gas emissions. Theoretically, the combustion products are CO₂ and H₂O, which are the waste chemical that goes in the environment, instead, in a solar-driven conversion waste materials are turned into fuels and chemicals again. [2]

This conversion is achieved in a solar refinery, and these fuels, which can be produced in liquid or gaseous form, offer multiple benefit in terms of grid stability, energy security, compatibility with existing infrastructure, and climate change mitigation. [3]

Hydrogen, the most elemental fuel, has many attractive attributes, such as, clean burning since water is the product of combustion and can be efficiently converted back to electricity via fuel cells. However, H_2 lacks volumetric density and the difficulties to transport or storage such material are the reasons why hydrocarbon fuels are preferred. So, rather than utilizing solar-generated hydrogen directly as a fuel, its utility is much greater as onsite reactant for converting CO_2 to CH_4 or for generating syngas, heat or electricity[4]. Given the reason discussed above, reacting carbon dioxide with hydrogen not only provides an effective way to store CO_2 , but also produces a fuel that is easier to store, distribute and pairs well with the existing energy supply infrastructure.

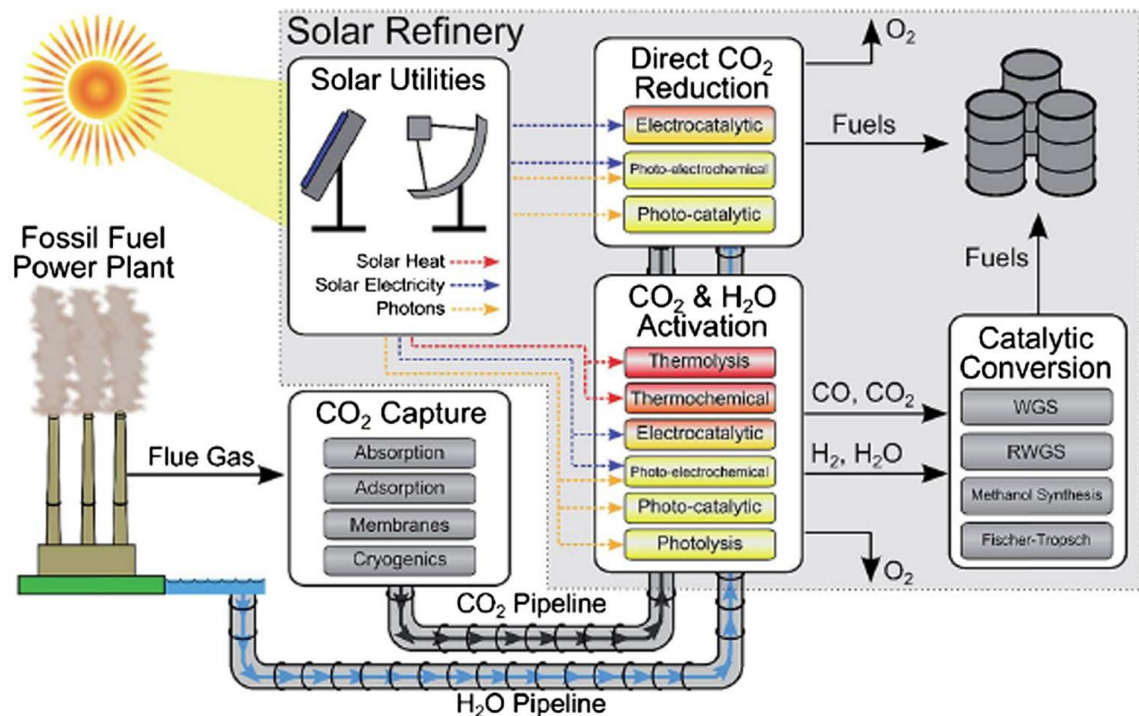


Figure 0.1.1 Schematic of a solar refinery and solar fuel feedstock [4]

1.2 Solar utilities

1.2.1 Technologies

Solar thermochemical process uses solar energy to feed high temperature endothermic chemical reactions. This kind of system is called solar furnace. The furnace is composed by a heliostat mirror that reflects the sunlight towards a concentrator which, in returns, diverts the beams into the focal point, where the reaction occurs.

There are two main layouts: on-axis and off-axis, the main difference is that, in the former, the focal point is placed in between the heliostat and the concentrator, instead, in the latter, it's not. Figures below shows a horizontal on-axis solar furnace and a vertical one.

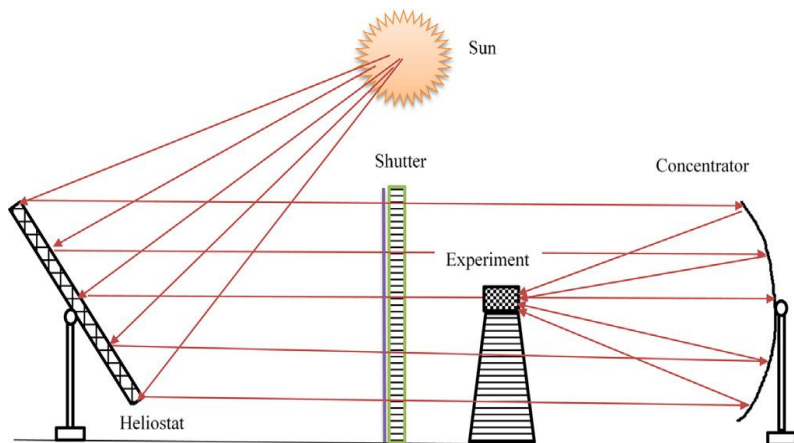


Figure 1.0.2 Schematic of a horizontal on-axis solar furnace [5]

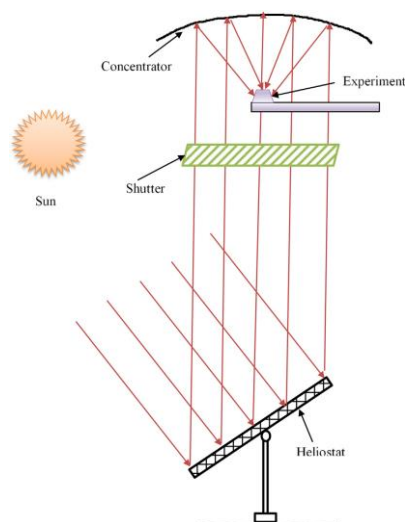


Figure 1.0.3 Schematic of a vertical on-axis solar furnace [5]

The advantage with this arrangement are symmetrical beams distribution away from the focal point and the option of reducing the solar radiation using a louver shutter [6]. None-the-less placing the experimental platform between heliostat and concentrator blocks some of the incoming radiation, which is the main drawback of this setup. To address this concern, an off-axis solar furnace, Figure 1.4, is adopted in NREL (USA) and DLR (Germany) [5]. However, the problem of the off-axis is that the beam is asymmetrical in respect to the focal point hence the maximum optical performance cannot be achieved [6].

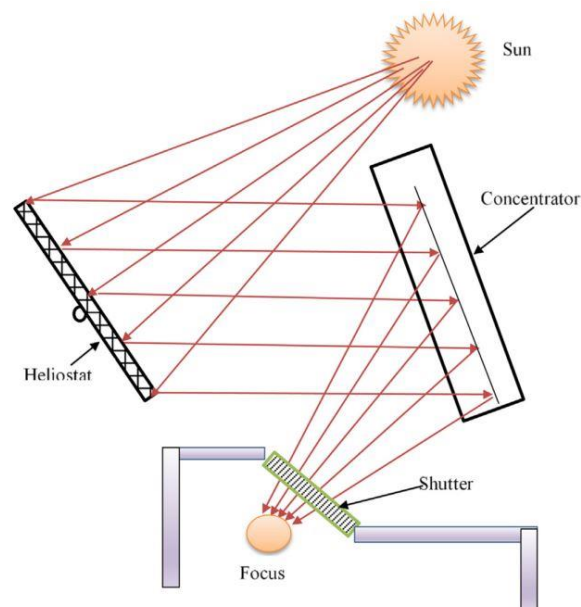


Figure 1.0.4 Schematic of an off-axis solar furnace [6]

Figure 1.4 shows how an off-axis solar furnace is assembled: the focal point is not adjacent to the heliostat-concentrator axis.

The solar furnaces usually are used for pilot scale demonstration, but for commercial scale solar thermochemical plant will use heliostat mirrors for high concentration and larger scale of operation. Hence, the design is taken from the solar thermal power plant, where a beam down system (Fig. 5) is proposed [6].

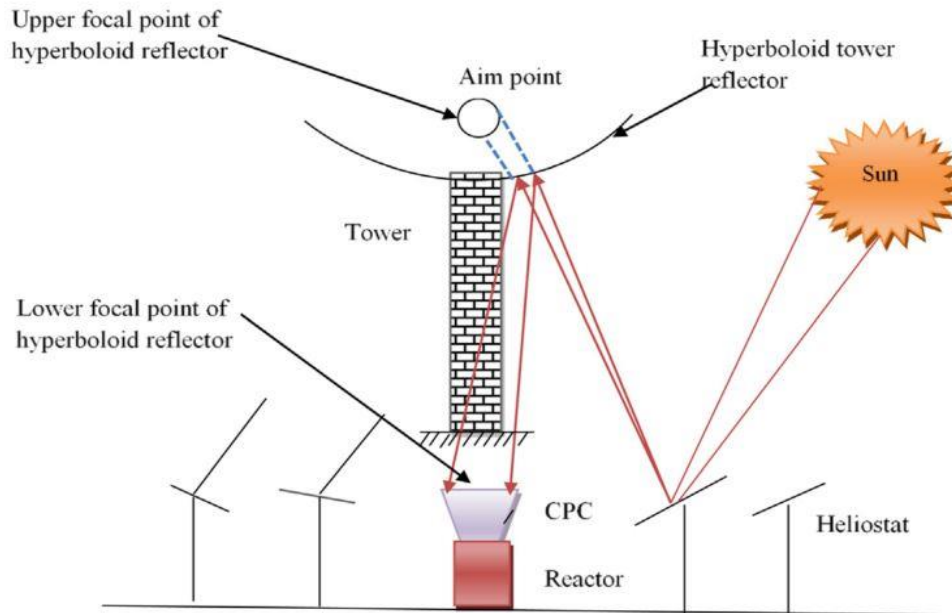


Figure 1.0.5 A beam down solar facility [6].

Using this kind of set, solar beam is reflected between the heliostat and the hyperboloid reflector and then is send to the reactor (on the ground). The position of the reactor simplifies the use and its maintenance [6].

1.2.2 Reactors

The reaction occurs inside the receiver, where the solar heat is collected. One of the categorization of solar receivers is done according to the mechanism of providing the solar heat to the heat transfer fluid, this can be done via direct or indirect receiver, the name of the first is Direct Irradiated Receiver Reactor (DIRR) and Indirectly Irradiated Receiver Reactor (IIRR) the second one. Another important distinction is done between reactors that perform only the thermal reduction, volatile cycle, and, reactors that do also fulfil the oxidation are the non-volatile type [6].

In the *volatile cycles*, due to the high temperature required for the thermal decomposition, the material involved often exceed the boiling temperature during the reduction phase. Thus, volatile redox pair employed usually exhibit a solid-to-gas phase at high temperature. This phase transition is thermodynamically positive for the process, thanks to the high entropy gain, but, in the other hand, though challenges occur due to recombination of the products of the decomposition reaction with the O_2 back to the

reactant in the product gas stream. Hence, a common problem of all these kind of cycles is how to avoid the recombination effect.

Non-volatile cycles employ redox pair oxides which remain condensed during the whole process, bypass the recombination issue discussed for the volatile cycles and include today a wide variety of single- and multi-metal, multivalent, metal oxide families. Since these material families remain in the solid state throughout the reaction their physiochemical characteristic such as specific surface area, particle size and porosity, become important for the realization of the reaction with gaseous steam/CO₂. However, the issue is not the production, but on whether the properties, porosity, particle size, active surface area, are maintained during the actual operation condition involving very high temperatures and repeated thermal cycling [6].

1.3 Thermochemical splitting of the water

The simplest pathway for thermochemical hydrogen production from H₂O is the direct/single-step water splitting. Figure 1.6 shows the Gibbs free energy change for direct thermochemical water splitting of the following reaction:



It equals zero at about 4300 K with ambient pressure. There are several issues during the development of a single step, solar-thermochemical water spitting process, such as,

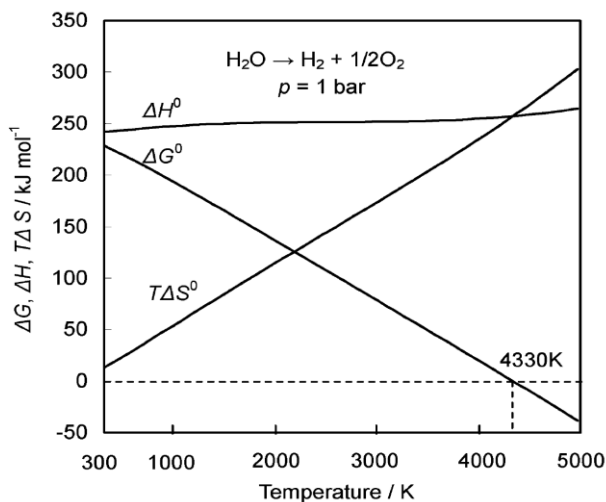


Figure 1.0.6 Variation of Gibbs free energy, Enthalpy and Entropy with respect to the Temperature [7].

the very high reactor temperature that has to be achieved through a secondary concentrator, hence increasing the system complexity. Special porous membranes that resist clogging by sintering due to high temperature involved must be developed to separate reaction

products. Recombination of products and intermediates (e.g. OH) must be avoided. These challenges to a single-step thermochemical water splitting process are not easy to overcome given the current state of the ceramic, solar and other technologies involved [7].

To lower the extremely high operating temperatures required and to remove the need for high-temperature gas separation, “multistep” thermochemical water splitting cycles started to raise up as a solution of those issues. In this work the focus in on the two-step water splitting process.

1.3.1 Two-step thermochemical cycles

The temperature of the direct thermochemical cycle may be avoided by introducing a redox pair material, in this way the single reaction splits in two more, a reduction and an oxidation, where the overall temperature do not get past 1500 °C. The trick of the metal oxide is to exchange oxygen ions during each phase of the cycle, in particular, during the reduction phase the metal oxide release part of its O₂, then, in the oxidation phase, it reacts with other species, such as water and carbon dioxide, grabbing oxygen from them; the metal oxide turn back in the original oxidation state, ready for the next reduction, while the water and the carbon dioxide are turned in hydrogen and carbon monoxide, respectively. The key characteristics of the material are the oxygen storage capacity, the temperature of the oxidation state changes, the rate of degradation and the reaction rate.

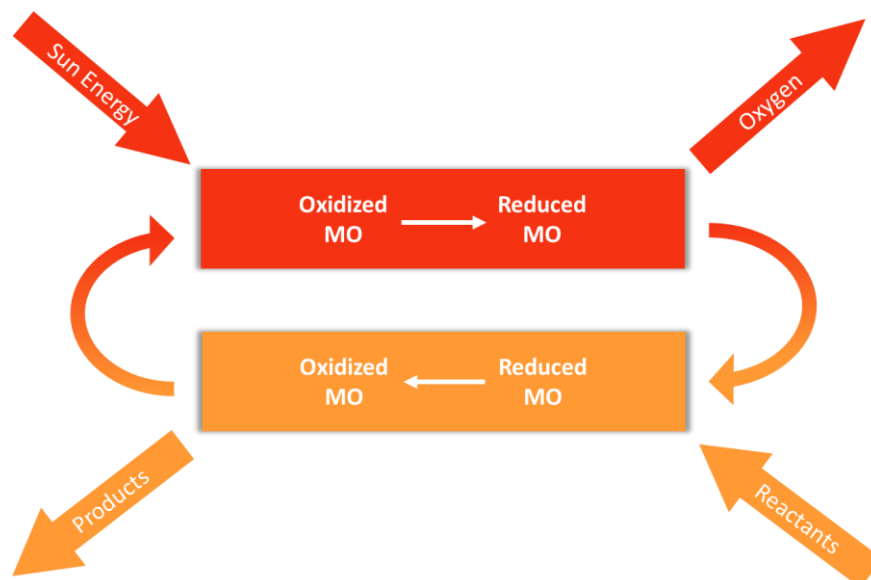


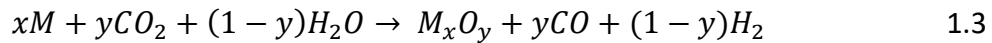
Figure 1.0.7 Scheme of the two-step thermochemical reaction.

The reduction step is described by the following:



The equation 1.2 describes an endothermic reaction taking place in the solar reactor. The metal can return to the metal state, if it's a volatile cycle, or, change its oxidation state back, if it's a non-volatile one. The reduction may also be performed by using hydrogen or methane with lower operating temperature and decreasing the time required to swing between higher and lower temperature due to the fast reduction kinetics, this become handy during the tests in laboratory.

The subsequent reaction is the oxidation step:



It is a general formulation for the syngas production and it can be performed also for water and carbon dioxide a part. This time there is an exothermic reaction and the temperatures required are lower [5].

Among the volatile cycles (solid-to-gas phase transition) the following are mentioned in the literature:

- **ZnO/Zn** is characterized by a combination of favourable thermodynamics properties, such as lower atomic weight and hence high energy content per mass, besides being not precious. However, the decomposition temperature of ZnO is at about 2300 K, whereas Zn melts at 692 K. Non-solar exothermic oxidation of Zn from H₂O and/or CO₂ has shown that the presence of inert ZnO affects both the oxidation kinetics and conversion of Zn. Diluent may have some positive effect on the conversion to Zn, in particular ZnO diluent generally increase it. Alternative approaches for the hydrolysis of Zn include aerosol flow reactor and hydrolysis by using nanoparticle [7].
- **SnO₂/SnO** have lower reduction step at approximately 1873 K from SnO₂ to SnO under atmospheric pressure, similar to the Zn counterpart there are some recombination effects, still, they can be reduced by using quenching devices as

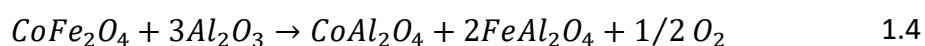
well as reduce partial pressure. The dissociation rate of the Tin is better than the Zinc and lower O₂ reactivity with respect to Zinc. Thus, better H₂ yield.

In this work the focus is on the non-volatile cycles:

- **Ceria cycle** and its well known CeO₂/Ce₂O₃ pair was used in the automotive sector as an oxygen system capable of store/release oxygen in oxygen rich/lean conditions, respectively. The first use of ceria was in the early '80s but the interest on this material, as a thermochemical cycles, was not revived until 2006 when dissociation of CeO₂ to Ce₂O₃ was achieved in solar reactor at temperature higher than 2200 K where ceria dioxide was already in the molten state. However much lower temperature is achieved reducing it at non-stoichiometric reduction (CeO₂ → CeO_{2-δ}), avoiding melting. The addition of cationic element M^{Y+} into the ceria structure was implemented to favour oxygen ions mobility during the reduction step. Ceria offers several benefits for thermochemical cycling over alternative metal oxide system: oxygen-deficient ceria shows very good reactivity with water and good hydrogen yield, but there are a known set of challenges, the most significant being the high TR reduction required [1]. Undoped ceria is an highly attractive candidate with inherent fast kinetics and superior crystallographic stability, making it the current benchmark material for compering the performance of new redox cycle for two-step water splitting [9]. Anyway, these aspects will be further discussed in the next chapter.
- **Ferrites' cycle** a whole series of ferrites was tested experimentally as well as studied for WS, including either one or two bivalent metal cation in the A site (Mn, Zn, Ni, Co). Their reduction temperature is in the order of 1600-1700 K, causing a serious sintering of the oxide. Attempt to lower the temperature using ZrO₂ in fine particle or support. Further, Fe ions dissolved within the Yttira stabilized Zirconia, YSZ, lattice are more "redox-active" than non-dissolved one leading to higher oxygen yield. With respect to materials composition, the current consensus seems to be that Zn- and Mn-containing ferrite exhibit volatilization and phase stability, respectively. Hence Ni/Co ferrite are the most

“robust” among ferrite. Notably, hydrogen production is more favoured in respect to CO production with the WS reaction being responsible for the 80% of the global FeO conversion [7].

- **Perovskites’ cycle** despite the fact this kind of material are well-known for their reversibility in delivering and picking up oxygen at high temperature from their application in fuel cell, perovskite did only recently attract significant attention for WS/CDS since 2013. Perovskite are a class of compounds that have this type of crystal structure ABO_3 , Lanthanum-Strontium-Manganese (LSM) $La_{1-x}Sr_xMnO_{3-\delta}$ and Lanthanum-Strontium-Aluminate (LSA) $La_{1-x}Sr_xMn_yAl_{1-y}O_{3-\delta}$ have quite good reduction extent respect to ceria. Different supports lead to different performance [7].
- **Hercynite cycle** is another spinel material family, the doped aluminum spinels of the formula $(A_xB_{1-x})^{+2}Al_2^{+3}O_4$ with A and B cation being Fe and/or Cu are used as thermochemical water splitters. A mixed cobalt ferrite-hercynite system was proposed by the researchers of the University of Colorado, USA, as an effective WS-TR system [8]. The hercynite occurred due to the reaction between $CoFe_2O_4$ and Al_2O_3 , with the ferrite deposited in the alumina support, at elevated temperature. In this case the redox pair reactions are the following:



With low thermal reduction temperature, thanks to the formation of more stable aluminates, that are more thermodynamically favourable than the formation of solid solution or vacancies [7]. The major limitation of hercynite cycle are the slow reaction kinetics [8].

2 SYNTHESIS AND CHARACTERIZATION

In this chapter I will discuss the process of synthesis and characterization of the material under investigation; thanks to the collaboration between *Politecnico di Torino and Università degli studi di Udine* I was able to work directly inside the chemical laboratory in Udine and, together to Prof. Marta Boero and Prof. Alfonsina Pappacena, we worked to make novel Ceria-Zirconia-Tin metal oxide. In particular, the synthesis of the samples were the white Ceria and the white Ceria-Zirconia, hence, without dopants and with different weight percentage, and then, Ceria and Ceria-Zirconia doped with Tin, always with different weight percentage.

2.1 The Sol-Gel Techniques

The sol-gel process provides an alternative pathway, with respect to the traditional synthesis through mechanical mixing, to the production of ceramic materials. The method employs appropriate precursors to make a colloidal suspension, called sol, which turns in to a tridimensional solid structure, the gel, thanks to hydrolysis and polymerization reactions. After that, drying and making a thermal treatment turns the gel in a ceramic oxide [10]. However, the solid solution of Ceria, Ceria-Zirconia and Ceria-Zirconia-Tin were prepared with a variation of this synthesis technique, in particular, using the so called Pechini Method [11]. The process differs from a standard sol-gel technique via citric acid by adding ethylene glycol.

Specifically, a complexation between metal cations, together with citric acid, and the ethylene glycol occur, then, the solvent (water), is left to evaporate. Once the solvent is vaporized there is the polyesterification reaction which bring to the formation of a rigid polymeric network preventing eventual segregation and/or precipitation, ensuring homogeneity to the final product.

The most important parameters for a good synthesis are the degree of acidity, pH, the amount of citric acid, CA, and ethylene glycol (EG) because those elements need some fine tuning in order to avoid oxide precipitation before the occurring of the polyesterification.

The condition utilized in this work are similar to [12], which are adapted to the preparation of ceria-based compounds. Here will follow the detailed description of the process.

The very first step is the weighing of the various ingredients that will take part in the reaction. The citric acid, which is in the form of a salt, is added in a crystallizer together with water, once the two components are well mixed the metal cation precursor needed for the rest of the reaction are poured inside the aforementioned becher. These operations are made at room temperature, and the mixing is ensured by a magnetic stirrer with its stir bar.

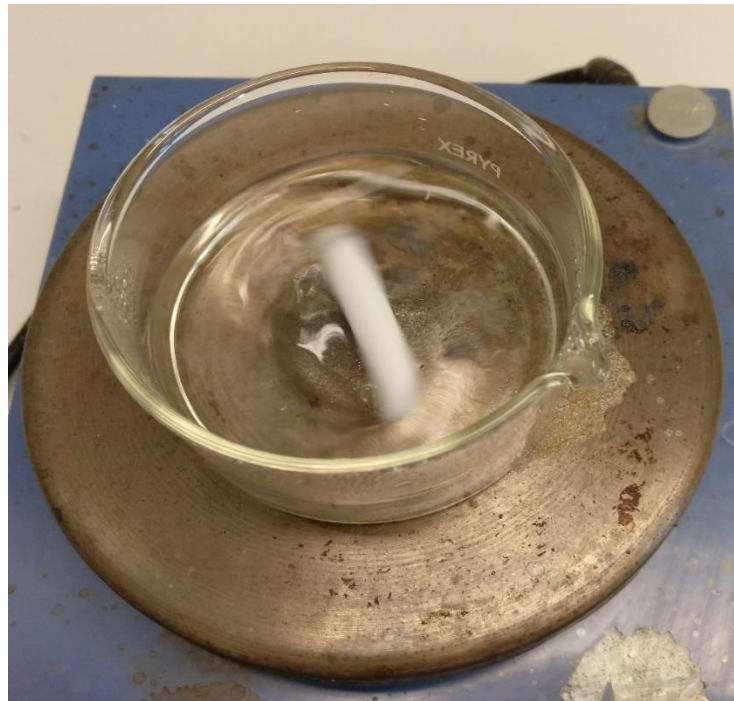


Figure 2.1 Solution of Ceria precursor in citric acid and water; The clearness of the solution indicates no metal precipitation.

At this point the temperature is increased at to the boiling point and the solution is left evaporate. Once the water is gone the polyesterification occurs, the gel became caramelized colour and much more viscous



Figure 2.2 The gel after the polyesterification.

Then the gel is removed from the becher and it's calcined at 400 °C for 6 hours. This initial calcination aims to remove any traces of undesired compounds; the remaining part is the ceramic oxide itself. The second thermal treatment, instead, aims to sinter the material at the future working temperature avoiding possible degradation of the material itself. In figure 2.4 is shown the comparison between before-after calcination.



Figure 2.3 Before after the first calcination treatment.

2.2 Calculations for the synthesis of catalyst

The preparation of the sample consists of the right doses of precursor, demi-water, citric acid and ethyl-glycol as a base, plus the precursor of zirconia and tin if the synthesis of Ceria-Zirconia or Ceria-Zirconia-Tin is performed. Hereafter a calculation example of a Ceria-Zirconia-Tin sample, which is the one that requires the bigger number of element in the solution. Keep in mind that the procedure is similar to all the samples except the difference in the amount of ingredients needed for less complicated oxide, i.e. in the ceria oxide the zirconia and tin precursors are not used.

Precursors and reactant utilized:

- Cerium Nitrate Exa-hydrate: $\text{Ce}(\text{NO}_3)_3 \cdot 6\text{H}_2\text{O}$
- Citric Acid Mono-hydrate: $\text{C}_6\text{H}_8\text{O}_7 \cdot \text{H}_2\text{O}$
- Zirconyl Nitrate: $\text{ZrO}(\text{NO}_3)_2$
- Ethyl Glycol: $\text{C}_2\text{H}_6\text{O}_2$
- Tin Chloride Dihydrate: $\text{SnCl}_2 \cdot 2 \text{H}_2\text{O}$
- Ethanol: $\text{C}_2\text{H}_5\text{OH}$

All reactants are provided by Sigma-Aldrich™ company.

2.2.1 Synthesis of Ceria Zirconia oxide doped with Tin

There is an example of calculation, the material chosen is a metal oxide with the following composition, $\text{Ce}_{0.8}\text{Zr}_{0.2}\text{O}_2 - 0.15\text{SnO}_2$. The stoichiometry indicates that the metal ion is composed by an 80% of Ceria and the other 20% by Zirconia, plus a 15% in weight of Tin oxide. The final mass of 1.5g is chosen for every catalyst, hence, all the calculations are done in respect of that mass.

The molecular weight of the $\text{Ce}_{0.8}\text{Zr}_{0.2}\text{O}_2$, which is calculated in the following equation:

$$PM_{CZ80} = 140.116 \cdot 0.8 + 91.224 \cdot 0.2 + 15.999 \cdot 2 = 162.34 \quad 2.1$$

The precursor weight is calculated by dividing the final mass of the catalyst by the 2.1 and by the weight percentage of Ceria inside the CZ80 times the molecular weight of the precursor $PM_{\text{Ce}(\text{NO}_3)_3 \cdot 6\text{H}_2\text{O}}$: 434.23 g/mol.

$$\frac{1.5}{162.34} \cdot 0.8 \cdot 434.23 = 3.21 \text{ g} \quad 2.2$$

Just like the ceria, the preliminary calculus for the Tin is done. Taking in to account the molar weight of the tin precursor $PM_{\text{SnCl}_2 \cdot 2\text{H}_2\text{O}}$: 225.65 g/mol.

$$\frac{1.5}{162.34} \cdot 0.15 \cdot 225.65 = 0.313 \text{ g} \quad 2.3$$

Tin is dissolved in 8 ml of ethanol before pouring in the becher with the rest of the solution. The mole of the oxide and the mole of the tin are paired up getting the mole of metal ions needed for the following reactions:

$$\frac{1.5}{162.34} + \frac{1.5}{162.34} \cdot 0.15 = 0.01063 \text{ mol} \quad 2.4$$

In complexation reaction must take in to account that AC ions have to be in the ratio 1:2 on the acid ($M^+/\text{CA} = 1/2$), as a consequence, using PM_{AC} : 210.1 g/mol

$$0.01063 \cdot 2 \cdot 210.1 = 3.88 \text{ g} \quad 2.5$$

The ratio for the polyesterification reaction must be $M^+/\text{EG} = 1/8$, which results, considering PM_{EG} : 62.07 g/mol:

$$0.01063 \cdot 8 \cdot 62.07 = 5.27 \text{ g} \quad 2.6$$

Since the EG is in liquid form a transformation through density and concentration is needed to calculate the exact amount of ml:

$$\frac{4.58}{1.113 \cdot 0.995} = 4.76 \text{ ml} \quad 2.7$$

Similar at what done for the ceria precursor, here follow the calculation for the weight of the zirconia, where PM_{ZrO_2} : 123.20 g/mol. The Zirconyl nitrate is in liquid form, so the concentration must be taken in to account.

$$\frac{1.5}{162.34 \cdot 0.236} \cdot 0.2 \cdot 123.20 = 0.965 \text{ g} \quad 2.8$$

Finally, the quantity of water is calculate taking in to account that 0.5 molar in respect to AC are used, so:

$$0.01063 \cdot 2 \cdot \frac{1000}{0.5} = 42.51 \text{ ml} \quad 2.9$$

2.2.2 Summary of the results

During the period in Udine I synthesized several catalysts, hence here follow some tables to clarify the quantity of sample prepared. After the synthesis of the white sample (CeO₂, CZ20, CZ50 and CZ80) the synthesis of the same sample with the different percentage of doping, for a total of a dozen of catalyst.

| White | | CO₂ | C20 | CZ50 | CZ80 |
|-----------------------------------|----|-----------------------|------------|-------------|-------------|
| Cerium Nitrate Exa-Hydrate | g | 3.785 | 0.979 | 2.205 | 3.210 |
| Zirconil Nitrate | g | | 4.710 | 2.651 | 0.965 |
| Tin Chloride Dihydrate | g | | | | |
| Ethyl Glycol | ml | 3.908 | 5.057 | 4.555 | 4.143 |
| Citric Acid Mono-Hydrate | g | 3.661 | 4.737 | 4.266 | 3.881 |
| Demi Water | ml | 34.86 | 45.11 | 40.63 | 36.96 |

| 0.15 SnO₂ | | CeO₂ | CZ20 | CZ50 | CZ80 |
|-----------------------------------|----|------------------------|-------------|-------------|-------------|
| Cerium Nitrate Exa-Hydrate | g | 3.785 | 0.979 | 2.205 | 3.210 |
| Zirconil Nitrate | g | | 4.710 | 2.651 | 0.965 |
| Tin Chloride Dihydrate | g | 3.785 | 0.382 | 0.344 | 0.313 |
| Ethyl Glycol | ml | 4.494 | 5.815 | 5.239 | 4.765 |
| Citric Acid Mono-Hydrate | g | 4.210 | 5.447 | 4.907 | 4.463 |
| Demi Water | ml | 40.09 | 51.88 | 46.73 | 42.51 |

| 0.25 SnO₂ | | CeO₂ | CZ20 | CZ50 | CZ80 |
|-----------------------------------|----|------------------------|-------------|-------------|-------------|
| Cerium Nitrate Exa-Hydrate | g | 3.785 | 0.979 | 2.205 | 3.210 |
| Zirconil Nitrate | g | | 4.710 | 2.651 | 0.965 |
| Tin Chloride Dihydrate | g | 0.492 | 0.636 | 0.573 | 0.521 |
| Ethyl Glycol | ml | 4.885 | 6.321 | 5.694 | 5.179 |
| Citric Acid Mono-Hydrate | g | 5.921 | 5.921 | 5.334 | 4.851 |
| Demi Water | ml | 43.58 | 56.39 | 50.80 | 46.20 |

2.3 Characterization of the Catalyst

The powders obtained were characterized in the chemical department of Udine, using the following techniques:

- Simultaneous Thermal Analysis (STA), is an analysis in which both the heat flow (DSC, Differential Scanning Calorimetry) and the weight change (TGA, Thermal Gravimetric Analysis) are measured, which give the right temperature to calcine the solid oxide;
- Brunauer-Emmett-Teller (BET), aims to determine the specific surface area, that is defined by ISO2012 as “the quantity of accessible surface of a sample when exposed to either gaseous or liquid adsorbate phase.”;
- X-Ray Powder Diffraction (XDR) is a technique used for identifying the structure of a crystal;
- Raman Spectroscopy gives more information about the structural transition after some thermal treatment.

2.3.1 Simultaneous Thermal Analysis

The measurement is performed by the SDT Q600, it provides simultaneous measurement of weight change and a true differential heat flow on the same sample from ambient temperature to 1,500 °C. It sponsors a field-proven horizontal dual beam design with automatic beam growth compensation, and the ability to analyse two TGA samples concurrently. DSC heat flow data is dynamically normalized using the instantaneous sample weight at any given temperature. Here follows a brief description of the steps to perform the measurement. The oxide powder is poured in the sample cap, usually 150 mg, then it's put down in the sample holder which in turn is supported by the balance arm. After this operation, the device starts, and the sample move inside the furnace. The furnace is placed horizontally, encased in a perforated stainless-steel enclosure. A stepwise isothermal approach is done, it consists of heating at a constant rate until a weight change begins (as determined by an operator-chosen rate) and then holding isothermally until the weight change is complete [13].



Figure 2.4 The SDT Q600 in the Udine Chemical Department during working operation.

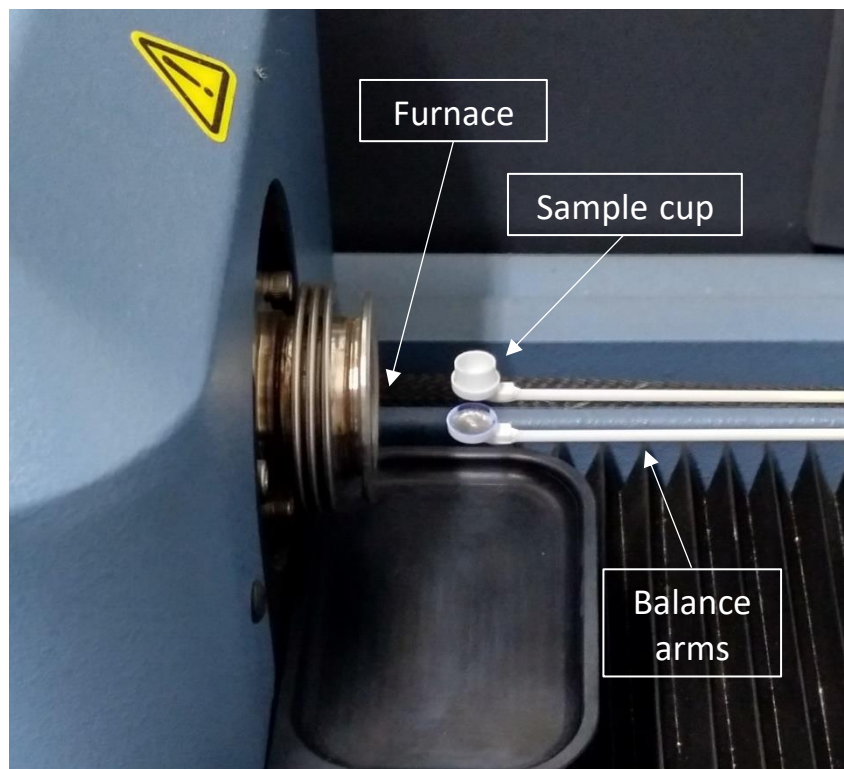


Figure 2.5 Particular of the preliminary operation for the STA session.

2.3.2 SDT Results

We evaluated the reduction extent of the materials at 1300°C in inert nitrogen. This kind of temperature similar to the one in the endothermic step during the thermochemical shift of the water, which bring to the hydrogen production during the second step, the oxidation phase, when the material enters in contact with the water.

The test is performed using 25 mg of sample heated to 1300 °C, using a ramp of 20 °C/min, then, is left iso-thermally for 80 minutes. The weight loss is experimentally associated to the reduction extent of the sample, the weight loss is relative to the loss of oxygen atom from the sample.

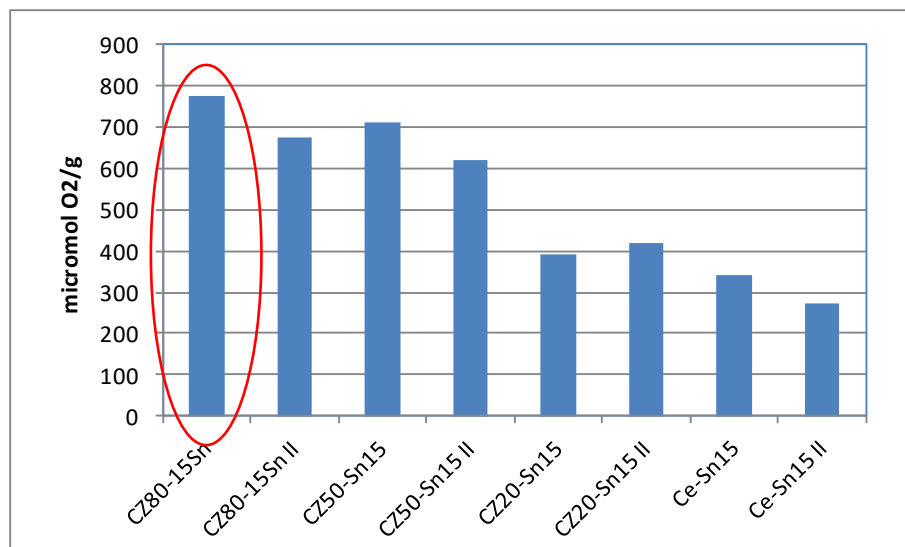


Figure 2.6 Reduction extent of the 15% weight Tin doped sample.

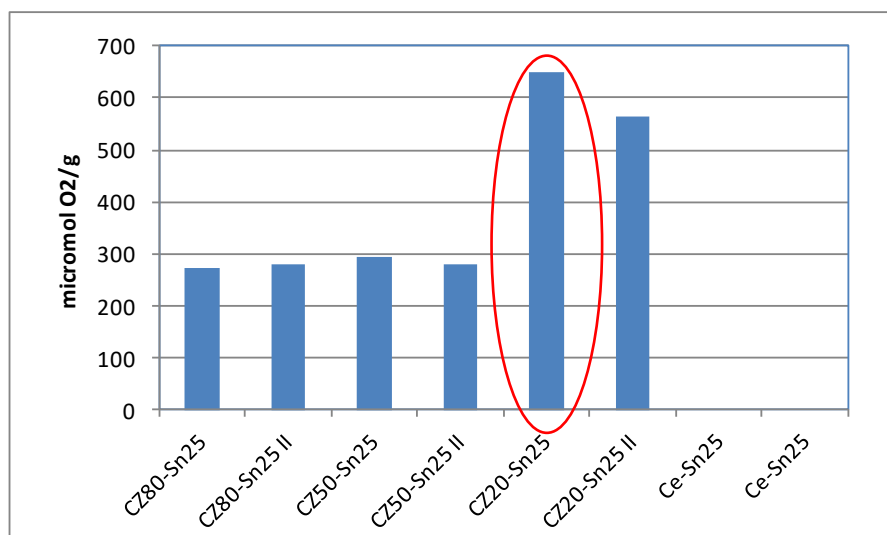


Figure 2.7 Reduction extent of the 25% weight Tin doped sample.

The figure shown the reduction extend, through the weight loss of the material. The highest two weight loss, meaning the highest reduction potential, are the CZ80-0.15SnO₂ and the CZ20-0.25SnO₂. These two materials are the ones chosen for further testing phase in the Torino laboratory.

2.3.3 Brunauer-Emmett-Teller

The scope of the BET theory is the quantification of the specific surface area of a given material. The specific surface area is defined as the surface area of a material divided by its mass or volume. Briefly, this method is based on the physical multi-layer adsorption of inert gases, such as, nitrogen, argon and carbon dioxide, on solid material to determine the specific surface area data [14].

The machine used is the TriStar 3000 by Micromeritics Corporation, this device allows three simultaneous measurement since it display three ports [15].

The experimental procedure consists in the warm-up of the device for about 30 minutes, in the meantime three sample are weighted, about 250 mg in specific glass holder. Afterwards the samples are placed in the instrument being evacuated and heated to get rid of the organic contaminants present. Then the sample are put in the sample tube together with a filler road and mounted in the analyser unit. The BET analysis starts by cooling down the samples to ~ 77 K, this is ensured by using a Dewar vessel filled with liquid nitrogen. The nitrogen injection under various pressure to determine the N₂ displacement for specific surface calculation.



Figure 2.8 Set-up procedure: heat under vacuum to erase organic trace.

The results of the BET are reported in the following table:

| Samples | SA [m²/g] | BJH desorption cumulative volume of pore [cm³/g] | BJH desorption average pore width [Å] |
|----------------|-----------------------------|--|--|
| Ce | 1.49 | 0.015 | 320 |
| CZ80 | 36.3 | 0.157 | 127 |
| CZ50 | 27.12 | 0.148 | 147 |
| CZ20 | 22.29 | 0.1 | 115 |
| CeSn15 | 27.31 | 0.113 | 130 |
| CZ80Sn15 | 26.82 | 0.181 | 209 |
| CZ50Sn15 | 30.75 | 0.134 | 115 |
| CZ20Sn15 | 32.7 | 0.141 | 117 |
| CeSn25 | 28.85 | 0.237 | 235 |
| CZ80Sn25 | 24.38 | 0.133 | 176 |
| CZ50Sn25 | 31.9 | 0.155 | 149 |
| CZ20Sn25 | 33.88 | 0.119 | 101 |

CeO₂ oxide is highly sintered, while CZ oxides preserve a surface area in the range of 22-36 m²/gr after a thermal treatment at 800°C/40 min. The thermal resistance is due to the insertion of Zr into the lattice of ceria. The surface area depends on the amount of Zr and the materials is generally characterized by adsorption isotherm of type H₂ with a distribution of pores in the range generally of meso- and macropores (>2 nm) depending on the compositions. CZ50 shows the largest distribution of pores.

The insertion of Tin is beneficial for the surface morphology of ceria. As the amount of tin increases the distribution of pores become broader and centered at values of 220-235 Å. Even if of minor entity, the same trends is observed for the CZ solid solutions, that showed subtle differences depending on their compositions.

3.2.4 X-Ray powder diffraction

Diffraction analysis can be done both using powder and denser materials, it exploits a predetermined wavelength, from parallel crystallographic layer, separated by a distance 'd'. The phenomenon is described by the Bragg law:

$$2d \sin \theta = n \lambda \quad \text{with } n \in \mathbb{N} \quad 2.10$$

If the incident radiation angle θ satisfies the above law, there is positive interference between diffracted rays that can be measured. Every peak returns an interplanar distance, from the analysis of those distances it is possible to identify the phase inside the sample using diffractograms. Schematic figure below shows the basic principle behind the Bragg law.

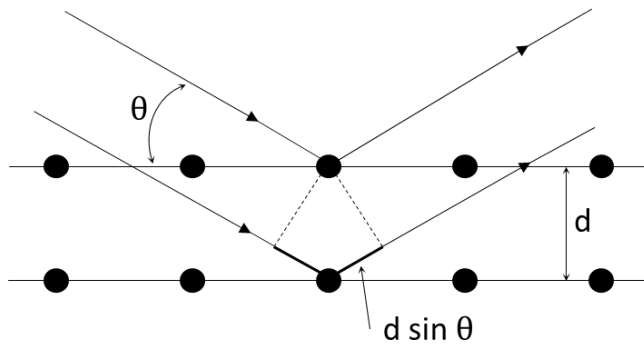


Figure 2.9 Working principle scheme of XRD.

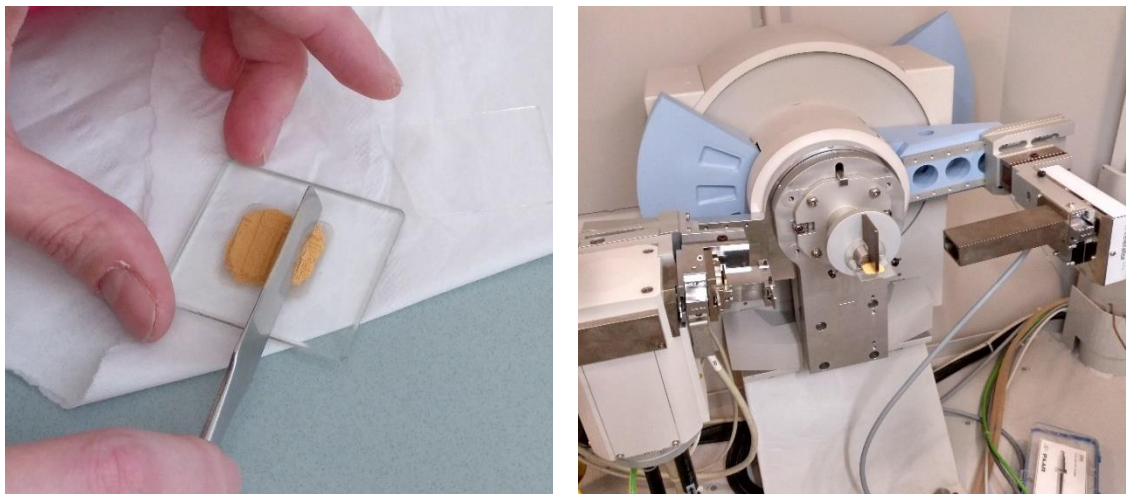


Figure 2.10 Setup procedure, preparation and measuring.

The sample preparation consists in filling a glass slide with the sample, as shown in figure. Then it is placed in the XDR housing, as show in figure.

In the analysis we recorded the spectrum using X'Pert powders diffractometer in the range of 20° and 90° θ , with a step of 0.02° and 40s acquisition time. The crystal phases are analysed with the Phillips software X'Pert HighScore [16].

The Ceria crystallised in the cubic phase. The synthesis of Ceria paired with Zirconia led to a solid solution, where the CZ80 crystallised in the cubic phase, while CZ20 and CZ50 in the tetragonal phase. The Tin doped materials, presents characteristic peaks of the Tin oxide, which also crystallise in the tetragonal phase, the more the Tin the more the peaks are visible.

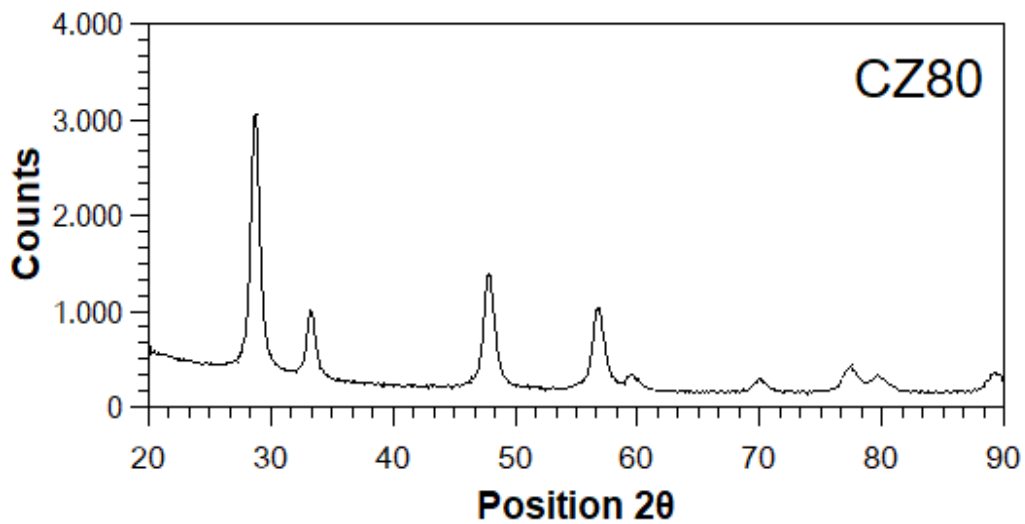


Figure 2.11 CZ 80 XRD crystal phase.

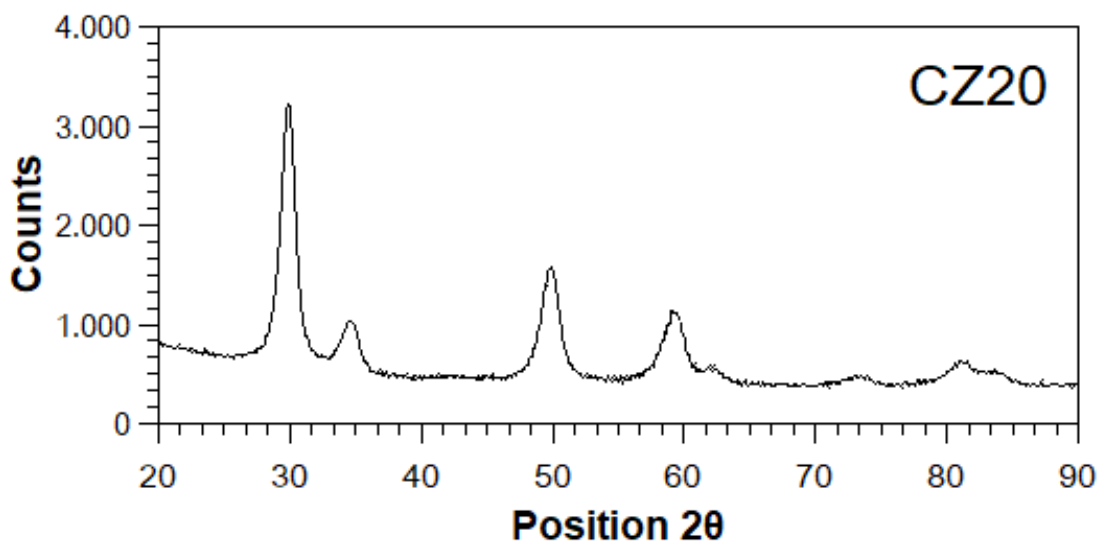


Figure 2.12 CZ 20 XRD crystal phase.

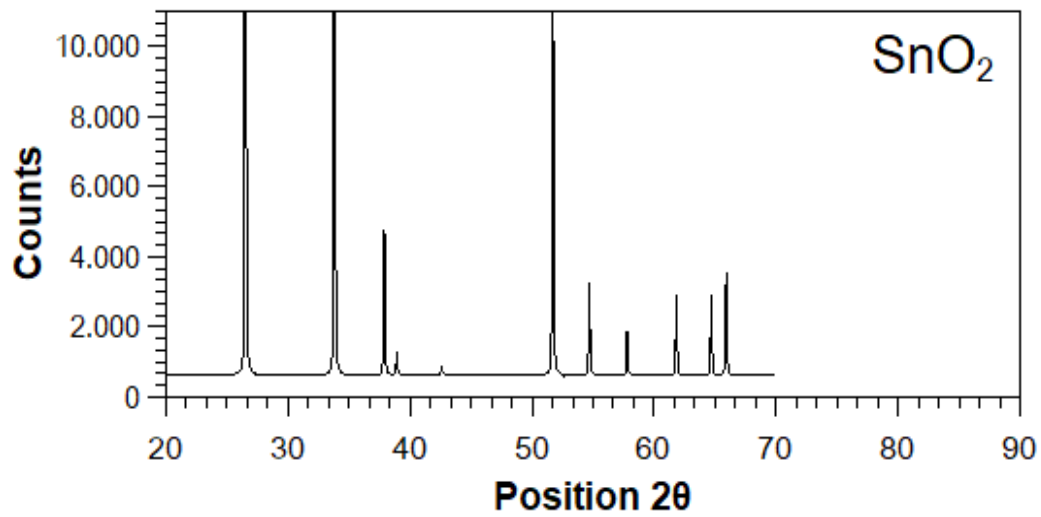


Figure 2.13 Tin oxide XRD crystal phase.

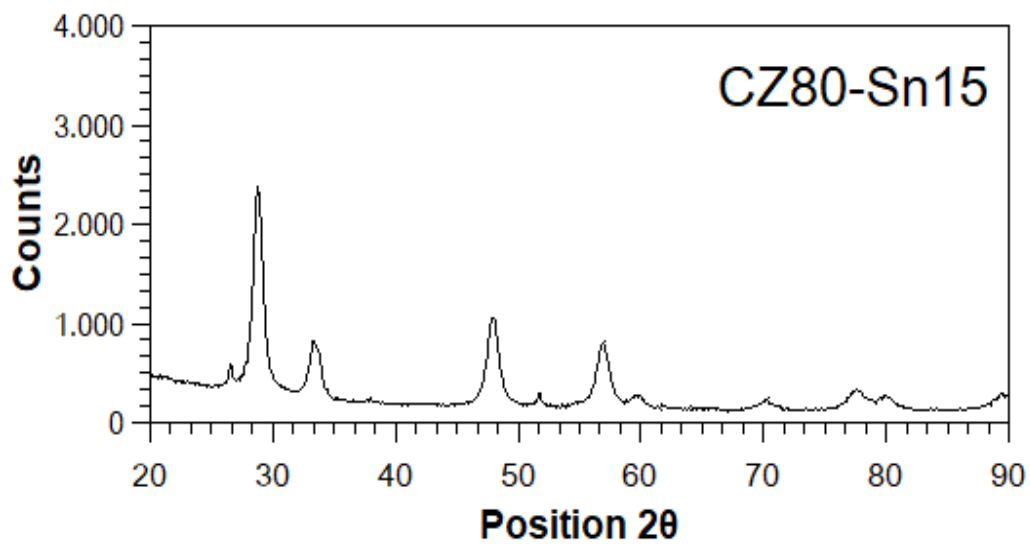


Figure 0.14 CZ80-0.15SnO₂ XRD crystal phase.

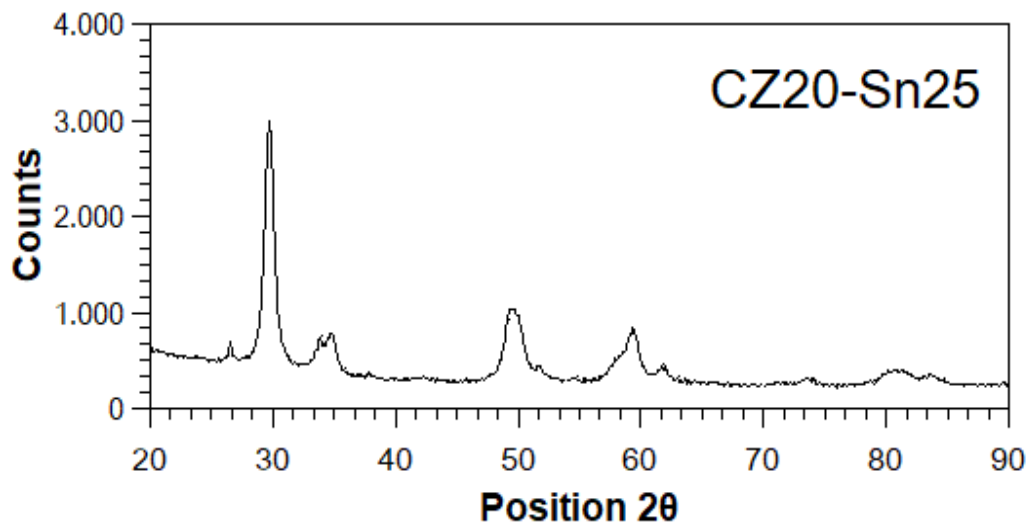


Figure 2.15 CZ20-0.25SnO₂ XRD crystal phase.

The figure 2. shown the peculiar peaks of the tin oxide, as expected, those peaks can be spotted also in the Ceria-Zirconia in the position 27° and 52° circa. The fact that the spectrum is, to a certain extent, made dirty by the tin is a good sign, indeed those added peaks make more oxygen vacancies that increase the reduction extent of the material.

3 EXPERIMENTAL

A description of the experimental setup employed for the test procedure is given followed by a review of the characteristics and working principles of the devices used.

3.1 Water splitting reaction tests setup

The aim of the water splitting test is to evaluate the hydrogen yield from the oxidation reaction of the metal oxide tested. The procedure leads to which sample is the winner in the range of the chosen synthesized material. The experimental system is suitable for both fuel-aided reduction and the thermal reduction.

The gases utilized for the tests are stored in cylinders. Once needed, the gases are sent to the line using electronic mass flow controllers, which are computer regulated using the LabView software. The mass flow is calibrated by the use of a mass flowmeter since the indicated flow on the mass flow controller display was often incorrect, the procedure consists of setting the wanted mass flow in the mass flowmeter, that is a device able to detect the amount of mass flow, then, adjust the flow in the mass flow controller in order to get that target measurement. The choice of the diluent is affected by the working principle of the mass spectrometer, indeed, the measurement device is not able to feel the difference between two molecules having similar molar mass, but since the hydrogen is the only compound measured there was no issue in choosing nitrogen as an inert diluent and as a purging gas.

The furnace is a horizontal tubular model, which is thermally controlled by the Eurotherm controller. The reactor is placed inside an alumina working tube, in the middle of the furnace, guaranteeing the right temperature, and the position is held thanks to four holed refractory cylinders.

After the furnace-reactor assembly there is the water trap system. The trap is mandatory since the mass spectrometer needs only dry gases to work properly. It consists in a fixed bed of small silica spheres that are able to absorb water from the flushing flow. The SiO_2 slowly deteriorates during its dehumidification work so it has to be regenerated by heating it up in a furnace to allow the desorption of the water. A qualitative check to the

amount of moisture contained in the silica trap is possible thanks to the colour of the grains itself, which turns from orange, when fresh, to greenish, when too hydrated. A particle filter is set upstream the mass spectrometer to reduce as much as possible the impurities from the entering gas.

The measurement of the outlet mixture composition was first carried out by the X-STREAM gas analyser with a TCD sensor for the hydrogen, then, after a failure on the device, by the aforementioned mass spectrometer, the HIDEN HPR-20, based on quadrupole mass filter and two different ion detectors: Faraday and SEM (Secondary Electron Multiplier). The former is suitable for high percentage of the measured gas species in the mixture, the latter is suitable for small percentage or ppm amount.

The mass spectrometer is only active during the oxidation step to detect the H_2 yield and the H_2 peak in the gas mixture. In figure 3. the set-up scheme is presented with its relative pictograms.

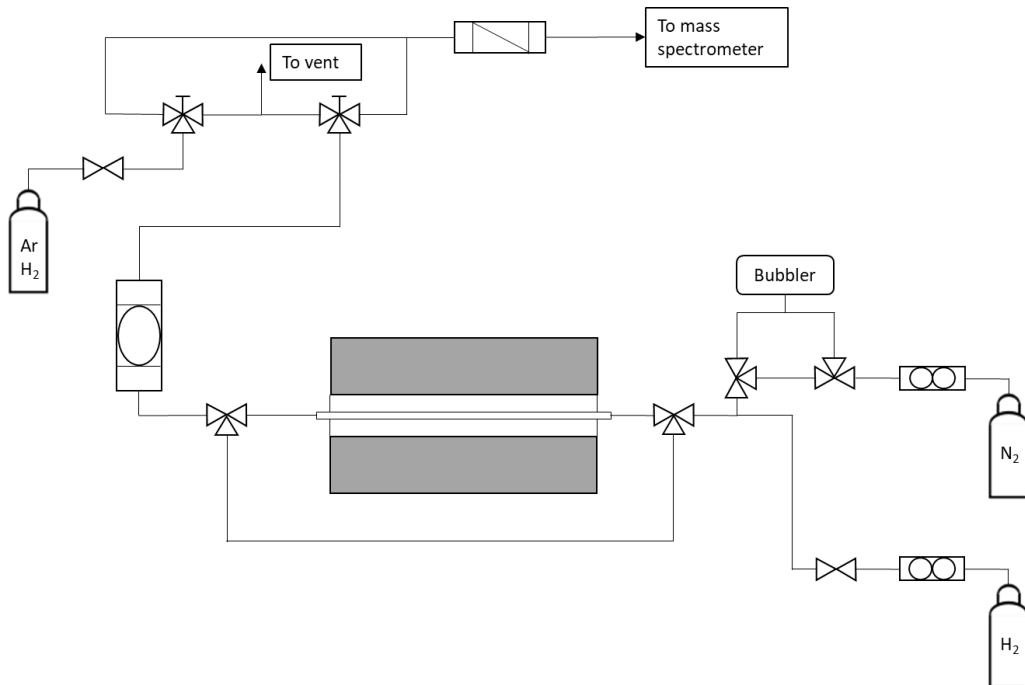


Figure 3.1 Scheme of the set-up.

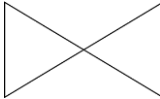
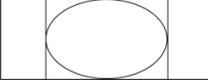
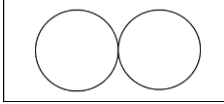
| Pictogram | Meaning |
|---|----------------------|
|  | Two-way valve |
|  | Three-way valve |
|  | Particle filter |
|  | Water trap |
|  | Mass flow controller |

Figure 3.2 Pictograms legend.

3.2 The furnace-reactor system

The reactions take place in the reactor that is placed into the furnace, the system is composed by two main components:

- Furnace (which provides the temperature needed for the reaction)
- Reactor (containing the fixed bed, where the reaction takes place)

The reactor is an alumina tube, it's 1m long, the inner diameter is 6 mm and the outer diameter of 10 mm, but both edges of the tube shrink the external diameter to 8 mm in order to better fit the connection with the others part of the system.

The horizontal fixed bed is made by introducing the catalyst powder within two fiberglass acting as a cap. Figure 3.2 shown the tube employed and figure 3.3 a schematic cross section of the fixed bed composition.



Figure 3.3 Top view of the alumina bar

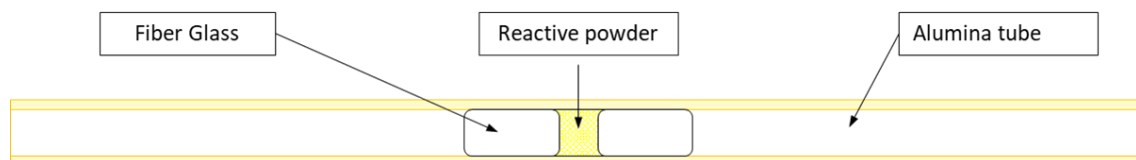


Figure 3.4 Cross section of the alumina bar

The oven employed is a tube furnace produced by Lenton Furnaces. The model is the LTF 16/50/180: the temperature reachable is about 1600 °C, an alumina tube of 50 mm inner diameter is the so-called work tube and the heated length is 180 mm long. The maximum power is 2500 W. The silicon carbide rod elements are placed parallel to the work tube and they provided heat. The efficiency and the stability it's maximised through the employment of low thermal mass insulation [17]. The global assembly is showed in figure 3.4, the blue basement contains also the control.



Figure 3.5 The furnace device, on the left side of the picture are shown the alumina cylinders that holds the reactor bar in the work tube.

3.3 TCD gas analyser

The first instrument used is the gas analyser from the Emerson Process Management. The X-STREAM XE is equipped with a sample gas pump, flow measurement with alarm, valve block, pressure sensor, digital input/output cards and an analogic input card. The analyser supports up to five analogical outputs, which, however, do not always need to be assigned to measurement channels which are physically present, if a unit features less than five channels, the remaining line can be used to transmit concentration levels with a different resolution [18].

In our setup, however, we used one single channel for the hydrogen. The other ones are for the methane CH₄, carbon monoxide CO, carbon bi-oxide CO₂ and oxygen.

3.3.1 Measuring Principles

Gas analyser supports several measuring principles depending on the gas of interest. This provides best possible results, as the measurement can be chosen to optimally fit the characteristics of the gas to be measured with respect to the application.

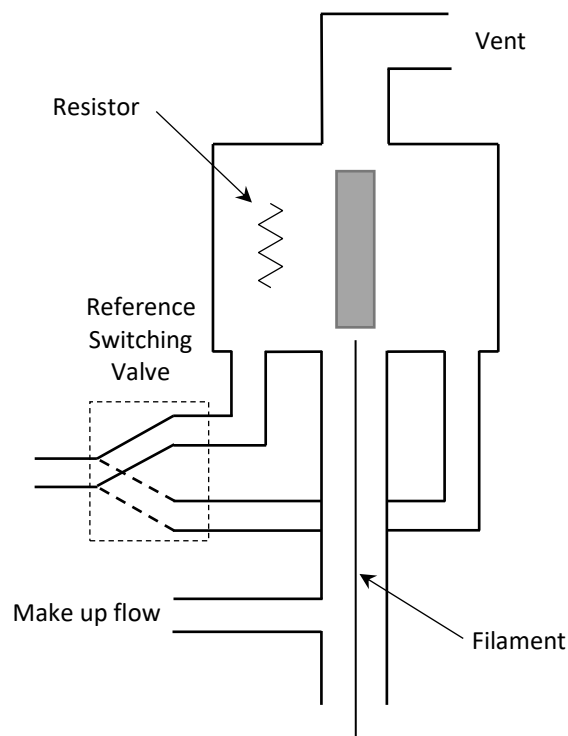


Figure 3.6 Scheme of a Thermal Conductivity Detector.

The TCD compares the thermal conductivities of two gas flows, the pure carrier gas and the carrier gas plus sample components. The detector contains a filament that is electrically heated, so it's hotter than the average detector body. The filament is kept at constant temperature while alternate streams of reference gas and column flow over it. When the sample is added, the power required to keep the filament temperature constant changes. The two gases stream are switched over the filament five times per second and the power differences are measured and recorded [19]. When helium (or hydrogen) is used as a carrier gas, the sample causes the thermal conductivity to fall, if instead, nitrogen is used the thermal conductivity goes up.

Infrared measurement (IR) and Ultraviolet measurement (UV)

The non-dispersive measurement methods utilize gas specific light absorption in order to discriminate between different gases. This is possible since any gas has its own absorption characteristic. This selective measurement of these absorption lines is a direct measure of the gas absorption. The amount of light absorbed by the absorption lines is a direct measure of the gas concentration [18].

There are two different types of non-dispersive measurement differing in the way the wavelength selectivity is accomplished. Typically, a gas selective detector is used for the NDIR measurement, the NDUV requires an additional filter.

IntrinZ Technology

The technology provides the reference measurement. In respect to the "proof peak" technology, it gives four reference measurement per revolution.

One important aspect of this patent technology is the fact the is not integrated in the measurement but, instead, is artificially inserted in the measurement signal. Frequency filtering separates the sum signal into measurement and reference signal, that results in a permanently referenced signal by dividing the integrated reference level by the integrated measurement level for each revolution.

This leads to very good features, such as the high dynamic measurement range, reduced temperature dependency and high sensitivity for lowest measuring ranges.

NDIR Detector

The standard detector used for NDIR measurement is an opto-pneumatic detector. It consists of two chambers, filled with gas and connected via a small channel. The filling gas is chosen to provide the maximum overlap with the to be measured, often the gas itself is used as a filler.

A micro flow sensor measures the flow between both the chambers. Once the light is absorbed by the gas in the absorption chamber, its temperature increase, increasing its volume. The gas expands and flows to the compensation chamber. When the chopper is closed, no light is absorbed and the gas temperature and volume tend to decrease. Then the gas flows back from the (now) hotter compensation chamber into the absorption chamber. The absolute flow, detected by the micro flow sensor, in both cases is therefore a measure for the light absorbed while the chopper is open. This directly correlates to the amount of light not absorbed in the analysis cell and therefore the concentration of the measured gas inside the analysis cell.

Using the divided analysis cell and the IntrinzX chopper wheel enables simultaneous detection of measurement and reference signal [18].

In Figure 3.7 a scheme of the NDIR detector is shown.

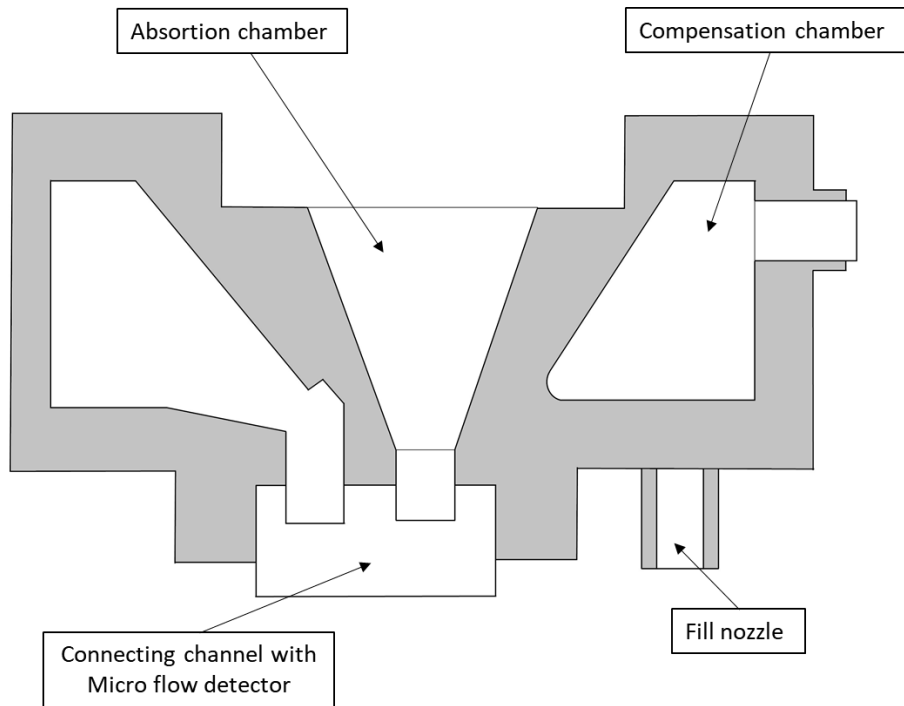


Figure 3.7 NDIR detector scheme.

Finally, a picture of the X-STREAM below.



Figure 3.8 Front view of the X-STREAM gas analyser.

3.4 Mass Spectrometer

The other type of gas analyser employed during the experiments is a HIDEN HPR-20 mass spectrometer. The mass spectrometer is able to detect the gas composition during time. The composition of the stream is self-extrapolated thanks to the similarities between partial pressure and molar fractions.

Its working principle is the ionization of gas molecules and control the ions pathway by applying an electric and a magnetic field. Due to the high reactivity of the charged molecules the device is forced to operate in vacuum condition, in the 10^{-5} ÷ 10^{-8} torr range, indeed, without vacuum the ions could lose its charge due to crash against atmospheric gases.

The HIDEN mass spectrometer is composed by three main components:

- Ion source
- Quadrupole mass filter
- Detector

The arrangement of them is schematically shown in figure 3.9.

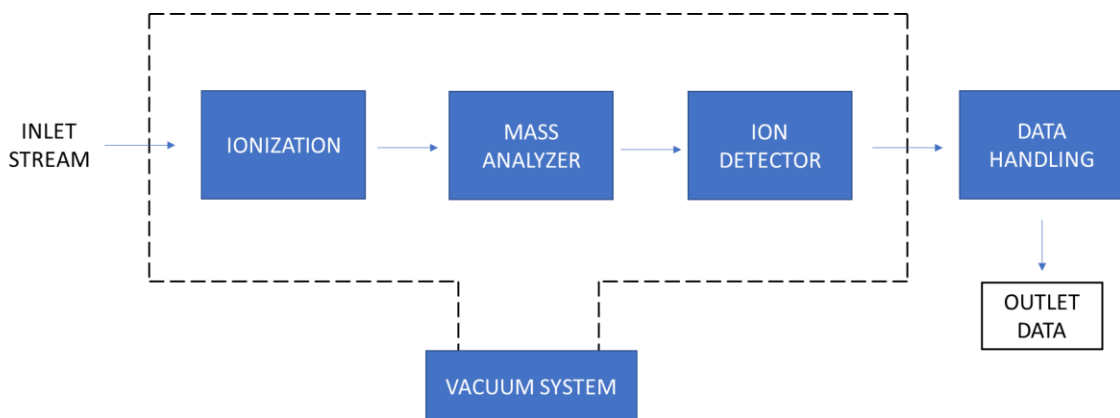


Figure 3.9 The working principle of the mass spectrometer

The ionization is the first step that occurs inside the mass spectrometer, here the gas molecules are hit by an electrons beam emitted by a hot filament, the kinetic energy involved causes the loss of an electron from the molecule. The phenomenon is described in the following equation:



Usually the instruments are tuned to work exclusively with positive ions, the latter may partially decompose producing fragment ions and/or neutral pieces. Each type of molecule has different characteristic and specific fragmentation depending by the molecule nature and by the operating condition.

By the application of a magnetic field the ions are accelerated, sorted and, on the basis of their mass and charge, they are divided in the mass analyser and finally detected. The results are collected on a chart, where a bar graph shows, for each mass/charge ratio detected, the amount of the corresponding ion through the height of the bar itself.

The ions produced have, usually, a single charge, so there is an equivalence between their mass/charge and the mass itself. As said before, the mass spectrometer works by imposing magnetic fields, hence the particle passing through the instrument are subjected to the Lorentz force, according to the equation 3.2:

$$\vec{F} = q \cdot \vec{v} \times \vec{B} \quad 3.2$$

Imposing the modulus of the Lorentz force equals to the centripetal force, we obtain:

$$q \cdot v \cdot B = m \cdot \frac{v^2}{r} \quad 3.3$$

The ion speed is correlated with the acceleration voltage through the:

$$\frac{1}{2} \cdot m \cdot v^2 = q \cdot V \quad 3.4$$

Merging equation 3.3 with the 3.4 is possible obtain the following:

$$\frac{m}{q} = \frac{B^2 \cdot r^2}{2 \cdot V} \quad 3.5$$

Where:

q is the ion charge [C]

v is the ion speed [m/s]

m is the ion mass [kg]

B is the applied magnetic field [T]

V is the applied voltage [V]

It follows that the application of certain values of magnetic field and voltage allows to isolate and detect a specific ion (with a specific m/q ratio).

3.3.1 Ion source

The most common technology employed in the ionization is the Electronic Impact Ionization. An incandescent tungsten filament emits an electronic beam. Electrons, which travel toward an anode (placed in front of the filament), gain high energy (around 70 eV). When these electrons come in contact with the electronical sphere of the molecules (electronic collision) there is an energy transfer that cause the expulsion of an electron with the formation of a cation. Since the transferred energy is higher than the energy required for the ionization, it is very likely that a further fragmentation occurs, with the formation of cation and radical. The positive ions are avoided by using a repellent plate toward a series of perforated plates, which have an increasing potential, in order to accelerate them. According to the equation 3.4, the kinetic energy of the ions exiting from the last plate is proportional to the voltage.

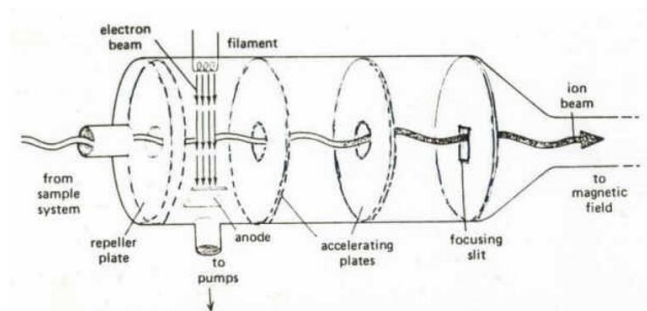


Figure 3.10 Scheme of EII source scheme [20].

3.4.2 Mass analyser

The technology of mass analyser moved from the use of magnetic field to gradually employ the quadrupole mass analyser, which working principle is the use of alternating quadrupole electric field.

The quadrupole is built by four cylindrical rods that border the path of the molecules coming from the ionization chamber and directing to the detector. These rods have an alternate electromagnetic potential in such a way that the vertical rods have positive potential and the horizontal negative one, or viceversa. The potential is in the form of $U + V \cdot \cos(\omega \cdot t)$, where U is DC voltage and cosine term is the AC voltage, the adjacent rod is 180° out of phase so the sign is opposite to the previous one. The electron coming inside the quadrupole get a zig-zag trajectory, since they are attracted by the positive potential but repulse from the negative one. However due to this unstable movement some of the electrons collide onto the bar, others, the ones with the right kinetic energy, turn into a sinusoidal motion and survive until the revelation system.

Hence, imposing different DC/AC value is possible to discretize specific mass/charge ratio that are able to reach the detector. This allow to obtain a mass spectrum by varying the rod voltage and monitoring the ions that are detected [22].

In particular, the voltage scanning may be performed with two techniques:

- U and V are kept constant, ω is varied
- U and V are varied, but keeping constant U/V ratio and ω

3.4.3 Ion detectors

The wide spread technology for the ion detectors employed in the mass spectrometer are the Faraday Cup detector and the Electron Multiplier detector, usually both of them are inside a single instrument since they are suitable in different conditions.

Faraday Cup

The Faraday detector is basically a metal cup, placed in a vacuum system, that intercept the ions beam receiving their charge, around 1.6×10^{-19} C. The cup is part of an electronic circuit. The current flow through the circuit it's accurately measured and it's directly proportional to the number of ions that are intercepted by the Faraday cup. A current of 1 nA in the circuit corresponds to the arrival of several billion singly charged ions per second at the metal cup. Thanks to the fact that the detection is based purely on the charge, the FC-based detectors exhibit no mass discrimination, which is an advance in high precision measurement. Errors in the current measurement are reduced with addition of an electron suppressor plate to the cup. The suppressor plate reduces losses thanks to backscattering of the incident ions and, also, it reduces the leakage probability for secondary electrons that may be released on ion impact. The limit of detection for a FC-cup is related to the sensitivity of the electrometer in the circuit that it is connected to. The current go through a circuit resistor in which a different potential is measured. Even though the current passing in the circuit is very low, often is necessary the employment of an amplifier that cause a "noise", the trade-off is that give a measurement time that can last several hundred seconds [21].

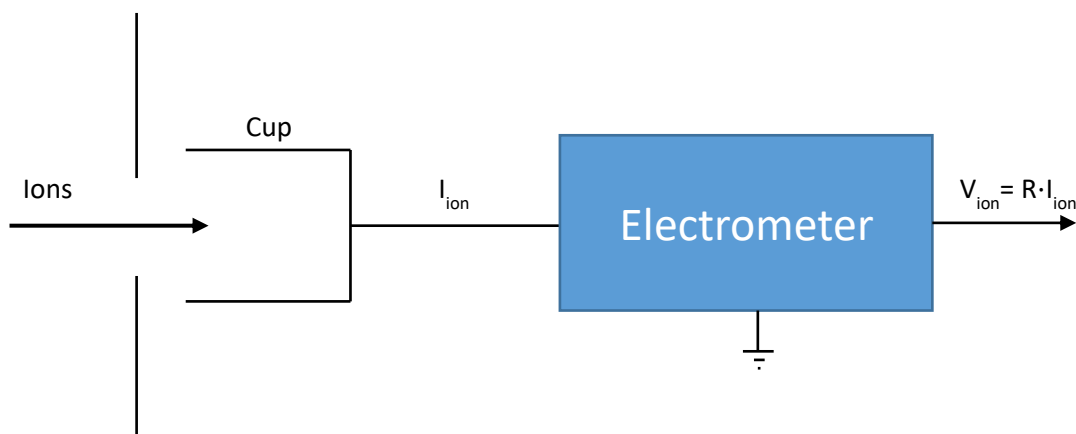


Figure 3.11 Scheme of Faraday Cup [20].

SEM

The acronym stands for Secondary Electron Multiplier, the basic physical process that allows this device to operate is called secondary electron emission. When a charged particle, ion or electron, clash a surface it causes a secondary electrons to be released from atoms in the surface layer. The number of new electron released depends on the type of incident primary particle, its energy and the characteristic of the incident surface. There are two basic forms of electron multipliers that are commonly used in mass spectrometry: the discrete-dynode EM and the continuous-dynode EM, the latter usually referred to as a channel electron multiplier of CEM.

The discrete-dynode EM is composed by a certain amount of dynode between 12 and 24 and the operation gain is in the range pf $10^4 - 10^8$. The figure 3.8 shows the secondary electron effect, the electrons are multiplied in the channel containing the dynodes until the electrometer [23].

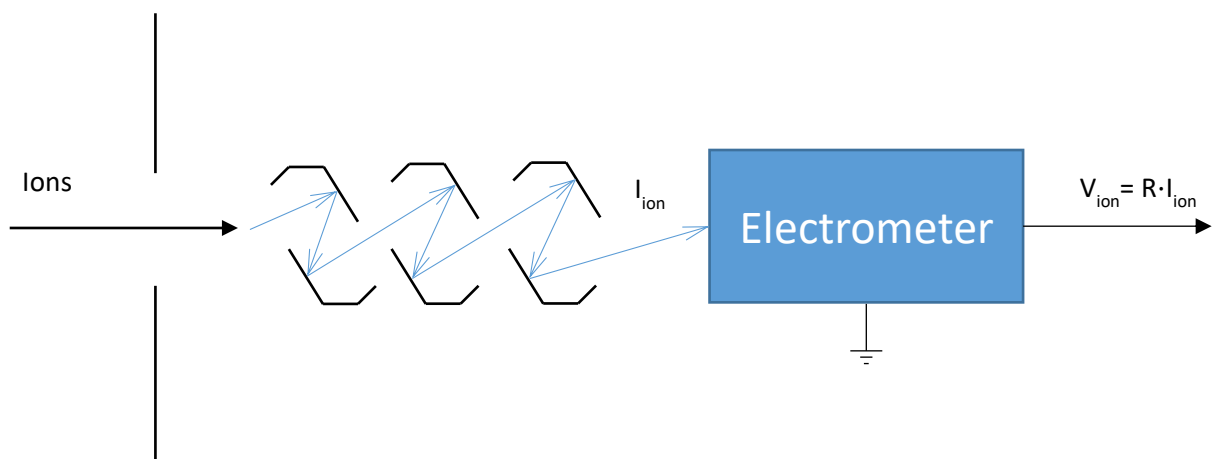


Figure 3.12 Scheme of discrete-dynode SEM, the blue arrows represent the multiplying effect that increase the ion current [22].

The continuous-dynode electron multiplier is feasible if the material of the electrodes has high resistance so that the function of the secondary emission and the voltage division are merged. This is often built as a funnel coated inside with a thin film of semiconductor material, with negative high voltage applied at the wider input end, and positive voltage to the other narrower edge. Similarly of what happens with the discrete geometry, electrons are made when the ion initially strikes the front of the dynode, then, the secondary electrons are accelerated towards the back of the detector by the potential drop, generating more electrons every time they hit the detector's wall. The increase in electron count is again exponential down the length of the detector. At the end of the funnel, electrons are passed into circuitry that give a signal to the software.

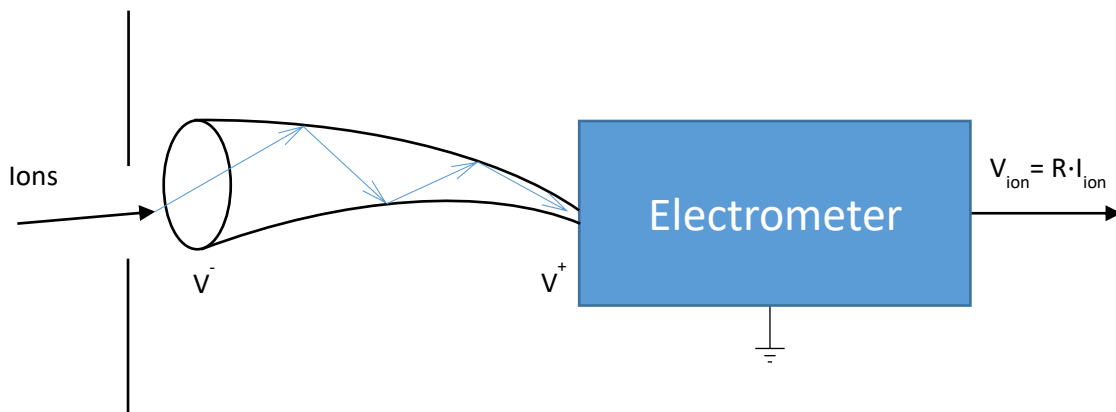


Figure 3.13 Scheme of continuous-dynode SEM, the blue arrows represent the multiplying effect that increase the ion current [22].

The mass spectrometer model employed is the HPR-20 QIC R&D produced by HIDEN Analytical. The device is equipped with both Secondary Electron Multiplier and Faraday Cup. It's designed to operate a continuous analysis of gases and vapours at pressures near atmosphere and it has a mass range of 200 AMU plus a detection capability from 100% to less than 5 ppb. The core of the system is the HAL 3F Series Triple Filter Mass Spectrometer: an assembly composed by electron impact ionisation source, a prefilter, a mass selective primary filter (quadrupole type), post filter and finally the detection assembly, which is constitute by the dual Faraday and the secondary electron multiplier, in series.

The HPR-20 is not the only instrument involved, indeed, there are other equipment dedicated to the instrument functioning []:

- A penning gauge
- A 60 l/s turbo drag pump
- A quartz inert capillary QIC flexible inlet, heated to avoid condensation
- A backing and bypass scroll pump
- The housing (mass spectrometer chamber)
- A bypass control valve

The whole instrumentation suffers the presence of water, as well as, of solid pollutant. The safety measurement employed are basically a solid particle filter upstream and a water trap downstream the furnace system.

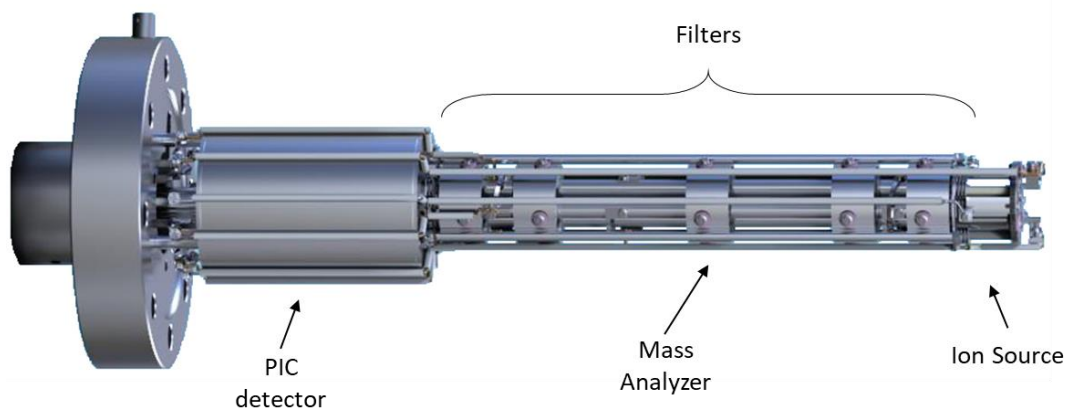


Figure 3.14 Mass Spectrometer assembly.

3.5 *Experimental procedure*

In this section the testing procedure followed for the experiments is described. The general procedure here described is the result of several refining step with respect to the initially adopted one, as during the months of tests we obtained a procedure that is well suited to proper record the hydrogen yield and its relative peak. Once get the data, which are represented in real time on screen, I was able to elaborate those in order to see how the material performs.

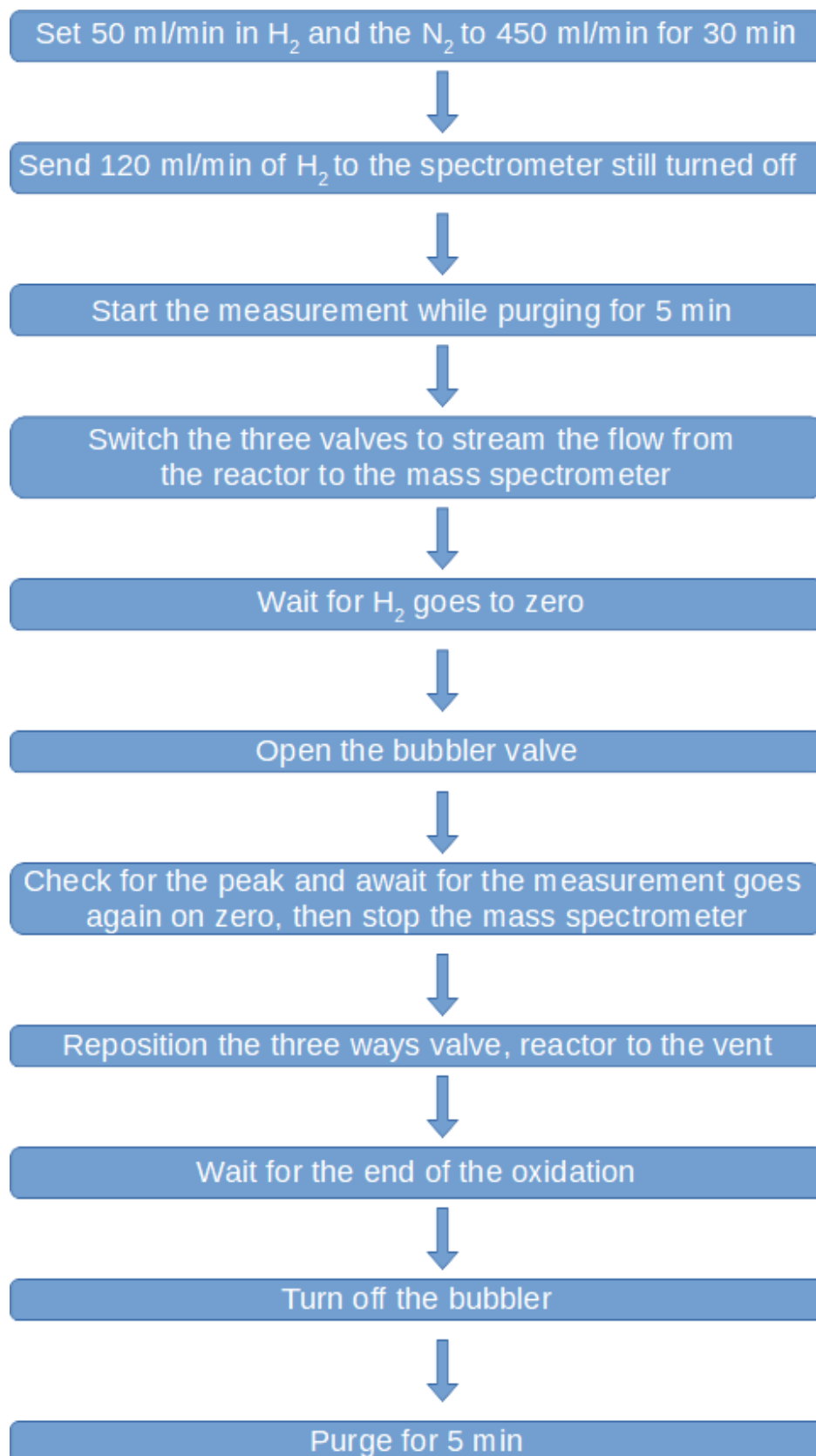
Each experimental test is based on a four-step cycle:

- **Reduction reaction:** a mixture of N_2 and H_2 at 5% of concentration in sent inside the reactor for 30 minutes, the total flow is 500 ml/min.
- **Purging step:** the hydrogen flow is removed, and the nitrogen flush the sample removing any trace of the previous step for about 10 minutes, the flow is reduced to 120 ml/min.
- **Oxidation reduction:** the bubbler valves are switched to add an additional steam flow, corresponding to roughly at 10% of H_2O in vapour phase.
- **Purging step:** the bubbler is shut down and a nitrogen flow wash the sample for another 10 minutes, the total slow is again increased to 450 ml/min.

The standard flow is 500 ml/min, during the test, instead, we realized that this amount of flow is too much for the spectrometer that cause a hardly peak, visual wise, this is not optimal since the real time plot gives us tool to detect if everything works well.

The most critical part is the first purging step. There are two fluxes in play, one is coming from the reactor and the other one is coming from the Ar- H_2 vessel (5% H_2). In this phase, the former goes to the vent, no measurement is needed, the latter goes to the mass spectrometer. The 120 ml/min flow from Ar- H_2 vessel ensures a steady detection of hydrogen to the spectrometer, which is crucial for having a calibrated value detected by the MS before the oxidation step, where is more difficult to keep track of the small amount of hydrogen produced in the reactor. In other words, sending H_2 before the actual measurement allows a better H_2 detection in the oxidation step, not only that,

the known flow of hydrogen is useful also as a reference measure for the later data elaboration.



3.6 Data Elaboration

The mass spectrometer software, in addition to the real time plot elaboration, returns also as an output a CSV files that can easily converted in excel file. The useful data are disposed in two column, which are time and pressure. From those to input we collected the data output of the wanted quantity, such as, hydrogen yield, time of conversion, reaction rate at the peak, or, information looking at the shape of the of the oxidation phase, i.e. if there is a narrow trend during the conversion, it means that the reaction is fast; if the trend is wider, the reaction takes place slower, those consideration give us a quantitatively idea of the sample activity.

In the figure is presented the raw data plotted.

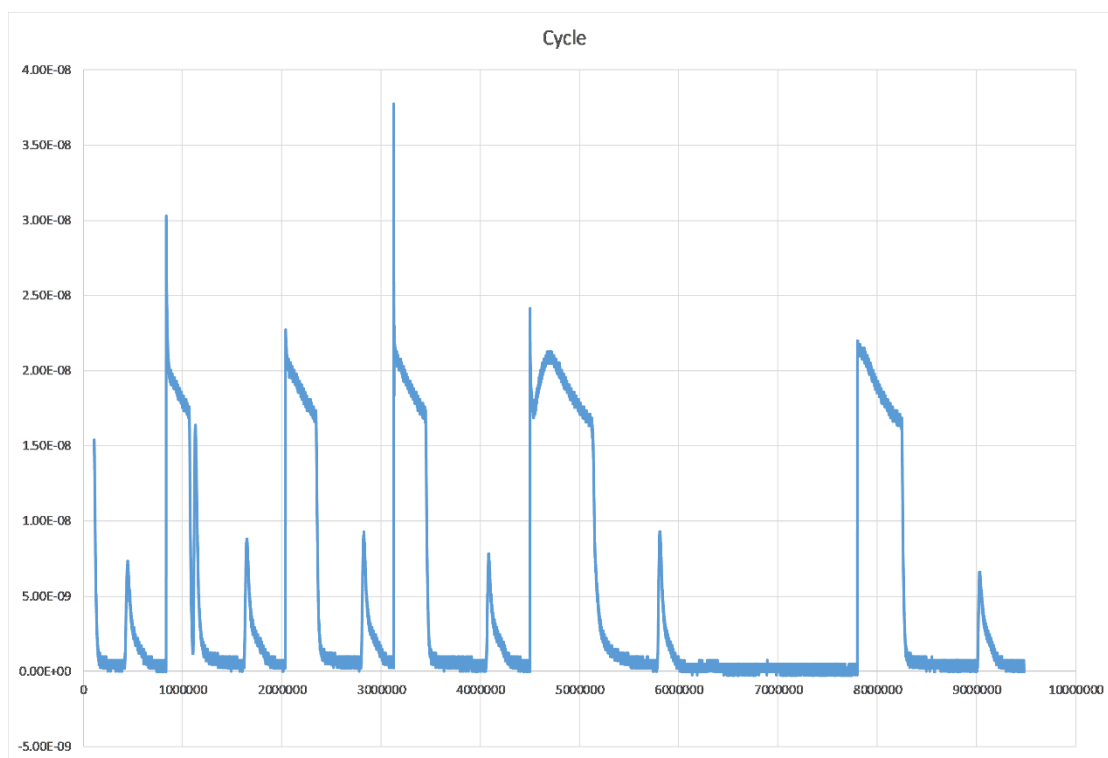


Figure 3.15 Hydrogen partial pressure measured by MS

The taller peaks are the measured hydrogen signals detected when the fixed Ar-H₂ flow is sent to the MS, so there is a known concentration of H₂ that corresponds to a certain partial pressure in the device. The smaller peaks correspond to the oxidation reaction where the hydrogen is produced; being the hydrogen fraction in the flow unknown this time, the productivity calculation is performed.

Then each purge-peak pair is calculated apart, let's focus on a single purge-peak pair, as shown in the figure below.

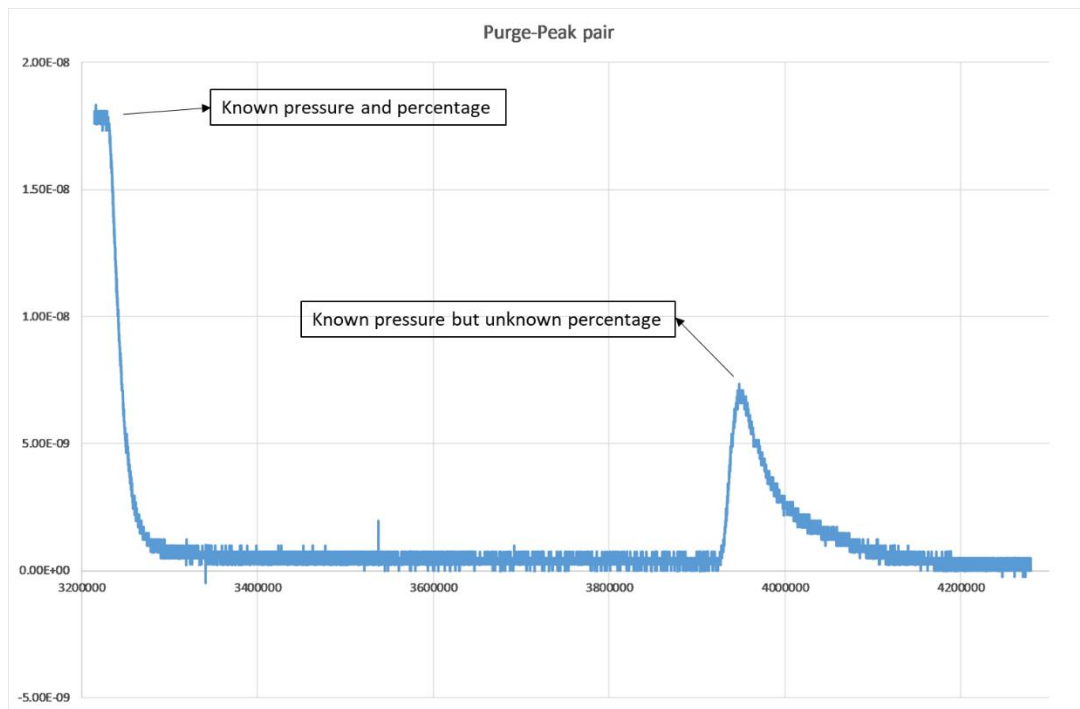


Figure 3.16 Purge-Peak pair.

The higher value represents the purging phase, where the three ways valves are turned in such a way that the reactor flow is still going to the vent, unprocessed, and the flow from the hydrogen vessel is going to the MS. Hence the mass spectrometer, in that moment, is measuring a pressure corresponding to 120 ml/min flow with known composition, that in turn gives a fixed H₂ percentage, since the pressurized vessel has a mixture of Argon and Hydrogen at 5%. When the measure is stabilized the valves are switched. Now the flow entering the device is the one from the reactor in purge phase, where there is no hydrogen, thus the measure goes down to near zero, and, as usual, we wait for the measure to stabilize. Then the bubbler valve are opened and the oxidation reaction takes place, eq. 1.3, the hydrogen is produced, as showed in the figure above with the production curve. As said before the mass spectrometer returns pressure as an output, but we need to calculate the amount of hydrogen produced. Through a simple proportion we can get the percentage of hydrogen in every single instant.

Hence to get the percentage the following equation is displayed:

$$H_2\% = \frac{H_2 \text{ pressure}}{\text{Purge pressure}} \cdot 5\% \quad 3.6$$

The eq. 3.6 returns the value of hydrogen pressure measured in a single instant.

In the spectrometer is flowing the base flow of nitrogen plus the hydrogen flow produced by the oxidation reaction, so, in principle, the total flow can be calculated through the:

$$\dot{V}_{tot} = \frac{120}{1 - H_2\%} \quad [ml/min] \quad 3.7$$

Subtracting the total flow with the known flow of nitrogen we get the net hydrogen flow, from here, adjusting the measurement unit to get mol/min we integrate in time to calculate the hydrogen yield.

$$M_{H_2} = \sum_{i=1}^n \dot{M}_{i H_2}(t) \cdot \Delta t_i \quad [mol] \quad 3.8$$

From the mole we can easy get the grams of hydrogen by multiplying for its molecular weight.

The peak rate and the conversion time can be calculated from the data, the former indicates the maximum rate of production, whereas the latter gives an indication of the duration of the oxidation reaction. Thanks to those quantities we are able to also have an idea of the reactivity of the sample, indeed, the sharper the peak, the faster the kinetics.

4 RESULTS

4.1 *Summary of the experiments*

The first sample tested was the CZ80 HSA, meaning HSA (High Surface Area), produced by Udine and not synthesized during the thesis. The aim of testing this oxide is the fact that its behaviour is known in the literature, so it was useful to us as a reference for the following materials, which behaviour is much less known. Further, it was particularly useful to become familiar using the instrument and thus, optimizing the experimental procedure.

The CZ80 HSA was tested formerly using a TCD gas analyser, different from the mass spectrometer used in the end. The gas analyser, as mentioned before was the Emerson X-Stream, and then we switched the measurement to the mass spectrometer due to TCD failure. The CZ80 HSA was tested in three different conditions, with no pre-treatment, pre-treatment in air and pre-treatment in nitrogen, while all the reduction phase was done by hydrogen reduction at 800 °C. Unfortunately, in the last test the device had a failure. The pre-treatment phase consists on thermal treatment at 1300 °C for four hours, the scope is to activate more the materials.

Using the MS we completed the first three tests on the CZ80 HSA. Then, for the next test on the CZ80 HSA, we performed a complete water split thermal reduction.

After the experiment on the CZ80 HSA we moved to the ones that I synthesized in Udine, the samples chosen were the CZ80-0.15SnO₂ and the CZ20-0.25SnO₂, since those showed a better activity and because we wanted to see the results by using high/low percentage of Ceria/Zirconia and the effect of the Tin percentage on the results. We both test the samples returning back on the hydrogen reduction, since, as a preliminary procedure, it's faster and more reliable in the production of results.

Finally, we tested also the CZ20, CZ50 and the CZ80.

In the following table a summary of the tests is presented:

| Analyser | Reduction | Pre-Treat. | Data | Note |
|---------------------------------|----------------|----------------|-------------|--------------------|
| CZ80 HSA | | | | |
| TCD | H ₂ | NO | 20-23/11/17 | ok |
| TCD | H ₂ | N ₂ | 24-30/11/17 | ok |
| TCD | H ₂ | Air | 01-20/12/17 | Instrument Failure |
| MS | H ₂ | Air | 08-12/01/18 | ok |
| MS | Thermal | N ₂ | 15-20/01/18 | ok |
| CZ80-0.15SnO₂ | | | | |
| MS | Thermal | N ₂ | 22-26/01/18 | ok |
| CZ20-0.25SnO₂ | | | | |
| MS | Thermal | N ₂ | 12-15/02/18 | Fail |
| MS | H ₂ | N ₂ | 28/02/18 | Fail |
| CZ80-0.15SnO₂ | | | | |
| MS | H ₂ | N ₂ | 12-16/03/18 | ok |
| CZ20 | | | | |
| MS | H ₂ | N ₂ | 26-29/03/18 | No reproducibility |
| CZ50 | | | | |
| MS | H ₂ | N ₂ | 30/03/18 | Fail |
| CZ80 | | | | |
| MS | H ₂ | N ₂ | 04-05/04/18 | No reproducibility |

4.2 CZ80 HSA: WS experiments with hydrogen reduction

The first tested catalyst is the Ceria-Zirconia 80, where HSA stands for High Surface Area. In the following table some physical and chemical properties are reported, in the figure the powder itself is shown. The former test is conducted without any thermal treatment, during the preparation set-up the sample is put as-it-is in the reactor. The particle size, meaning the average diameter is around 0-32 μm . Meanwhile the sample weight is set to 250 mg.

| | |
|-------------------------|--|
| Raw Formula | $\text{Ce}_{0.8}\text{Zr}_{0.2}\text{O}_2$ |
| Appearance | Light Yellow |
| Odour | Odourless |
| Melting point | 2200 $^{\circ}\text{C}$ |
| Molecular Weight | 162.3 g/mol |
| Relative Density | 6.2 g/cm ³ |



Figure 4.1 Visual look to the sample

4.2.1 WS results (TCD measure)

The overall cycle trend, for TCD, is shown in the figure 4.2, the calibration is done by using the signal of the 10% H₂ measured during the reduction phase of the sample with a mixture of H₂-N₂ with 10% H₂.

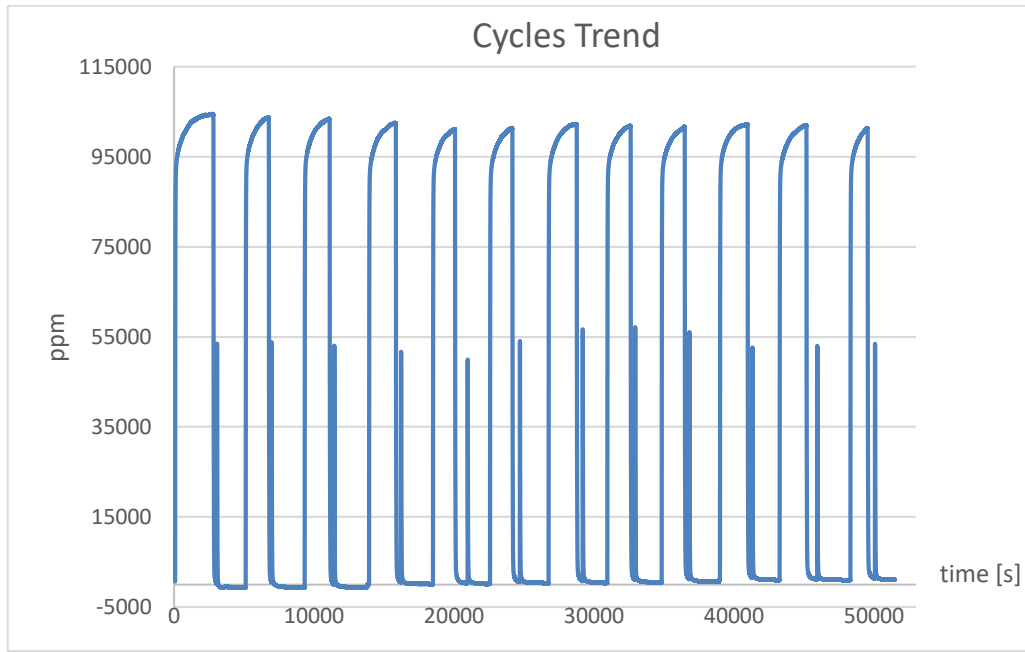
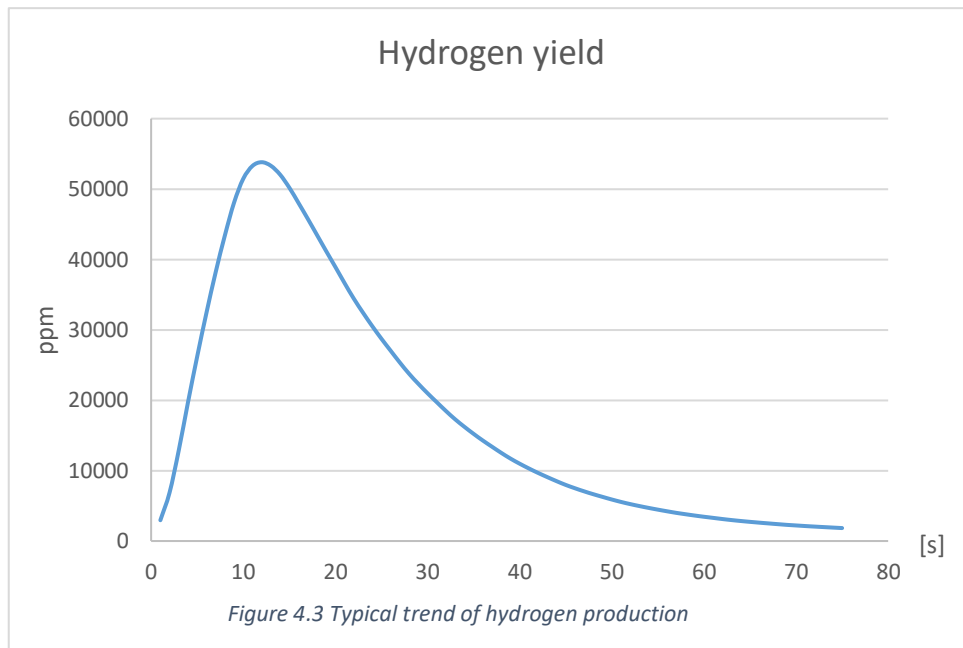


Figure 4.2 Overall shape of ten consecutive cycle.

As you can see, using the TCD, the hydrogen signal during the purging phase (the higher peaks on the graph) remains more constant during time and over many cycles. The measure is also a bit more reliable. The lower spikes are the oxidation phase, which is better shown in the figure below. One of the main advantages of this device is that the measure is directly the ppm of hydrogen in the mixture, which is then trivial to transform in more understandable unit of measurement. Thanks to the fact that the ppm is already reported there is no need of calculation similar to the calcs need using the mass spectrometer.

In the figure 4.3 is reported a single oxidation phase, where the hydrogen is produced.



The CZ80 HSA gave us remarkable results, although the peak and the hydrogen yield vary through every cycle.

The experimental set-up was the following:

Without nitridation the sample is heated in N_2 from ambient temperature to $800\text{ }^\circ\text{C}$ with a ramping phase of $10^\circ\text{C}/\text{min}$, each cycle is composed by four steps:

- **Reduction:** in H_2 at 10% for a mass flow of 50 ml/min H_2 plus 450 ml/min N_2
- **Purging:** in N_2 for 5' (total mass flow 450 ml/min)
- **Oxidation:** in H_2O at 10%, for a total mass flow of 500 ml/min.
- **Purging:** in N_2 for 5' (total mass flow 450 ml/min)

Regarding the pre-treatment, another sample of the same species is left for 4 hours at $1300\text{ }^\circ\text{C}$, this is the 'ageing' process known as nitridation, after that the sample follow the previous experimental campaign.

4.2.1.1 CZ80 HSA: effect of nitridation

The comparison consists to evaluate the difference in the behaviour between the sample tested using the nitridation treatment and the one with no pre-treatment.

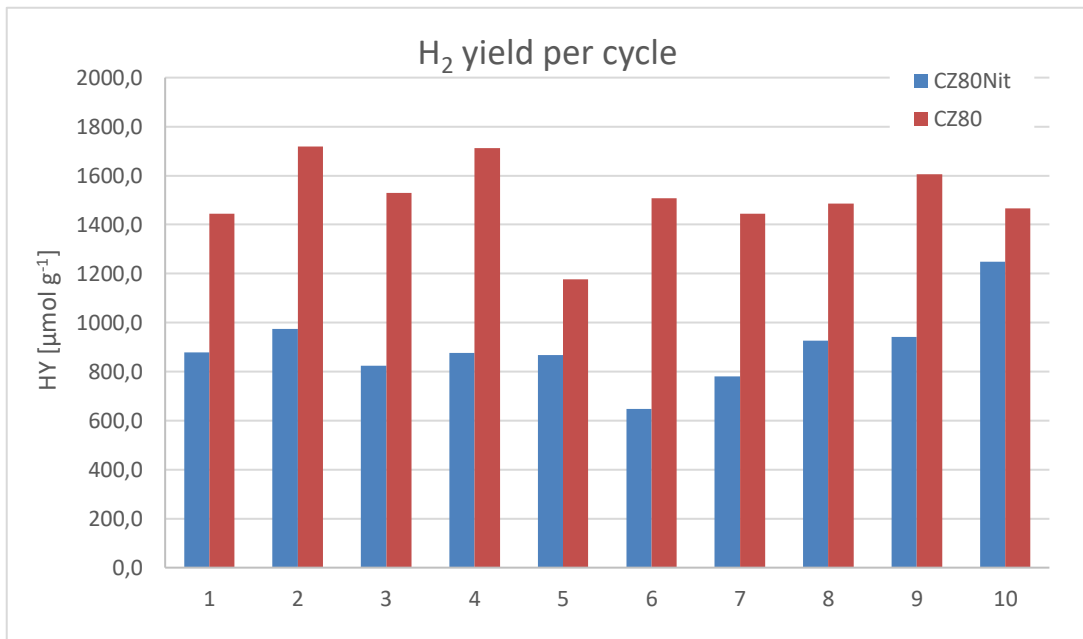


Figure 4.4 Hydrogen production comparison with and without thermal treatment

| | | | | | | | | | | |
|----------------|--------|--------|--------|--------|--------|--------|--------|--------|--------|--------|
| CZ80Nit | 879.5 | 975.0 | 824.8 | 876.0 | 868.1 | 647.4 | 779.6 | 927.4 | 941.4 | 1248.8 |
| CZ80 | 1443.8 | 1719.6 | 1528.5 | 1712.5 | 1176.1 | 1506.6 | 1445.6 | 1485.7 | 1605.2 | 1465.5 |

Table 1 Hydrogen yield value, measured in μmol g⁻¹

The results are composed in three main data, the conversion time (toc), the peak rate (PR), and, the most significant, the hydrogen yield (HY).

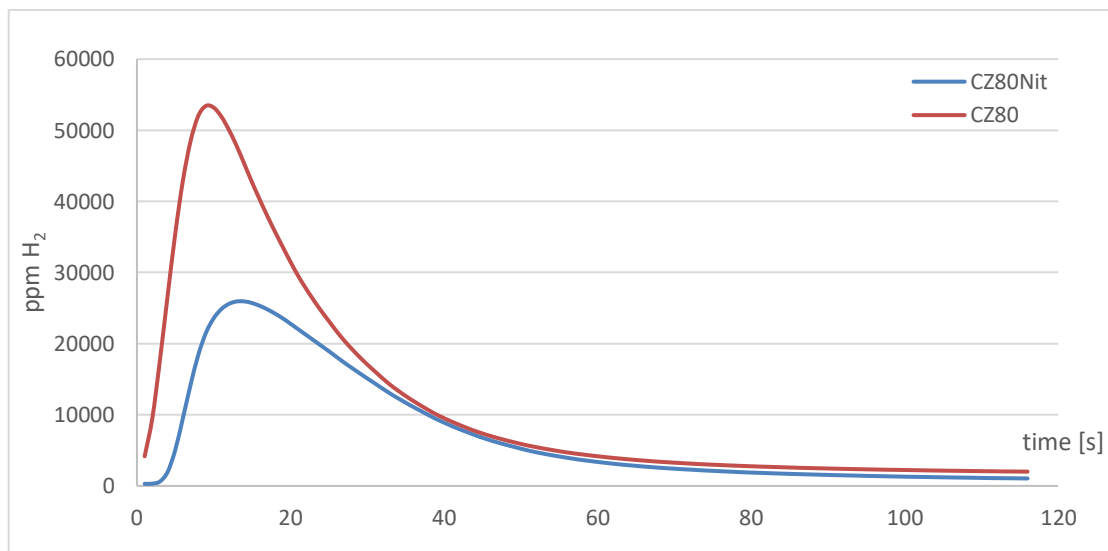


Figure 4.5 Different hydrogen production between thermal treatment

The yield of hydrogen is quite steady, and the nitridation got worse the H₂ production. None the less this thermal treatment is needed because it ensures a reliable and stable performance at higher temperature at which the metal oxide would be reduced in a real cycle. Indeed, the hydrogen reduction performed in these tests is not the realistic reduction method for the metal oxide in a real water splitting cycle, in which the metal oxide is thermally reduced at much higher temperature, in the order of 1300K.

The peak rate and conversion time are presented in figure 4.5, table 4.2 and 4.3.

| | | | | | | | | | | |
|----------------|-------|-------|-------|-------|------|-------|-------|-------|-------|-------|
| CZ80 | 105.0 | 106.6 | 106.1 | 102.3 | 99.9 | 108.0 | 113.3 | 105.9 | 112.1 | 105.3 |
| CZ80Nit | 43.9 | 55.8 | 52.6 | 48.9 | 53.2 | 45.4 | 56.0 | 57.2 | 48.8 | 51.9 |

Table 2 Peak Rate, measured in $\text{cm}^3 \text{min}^{-1} \text{g}^{-1}$

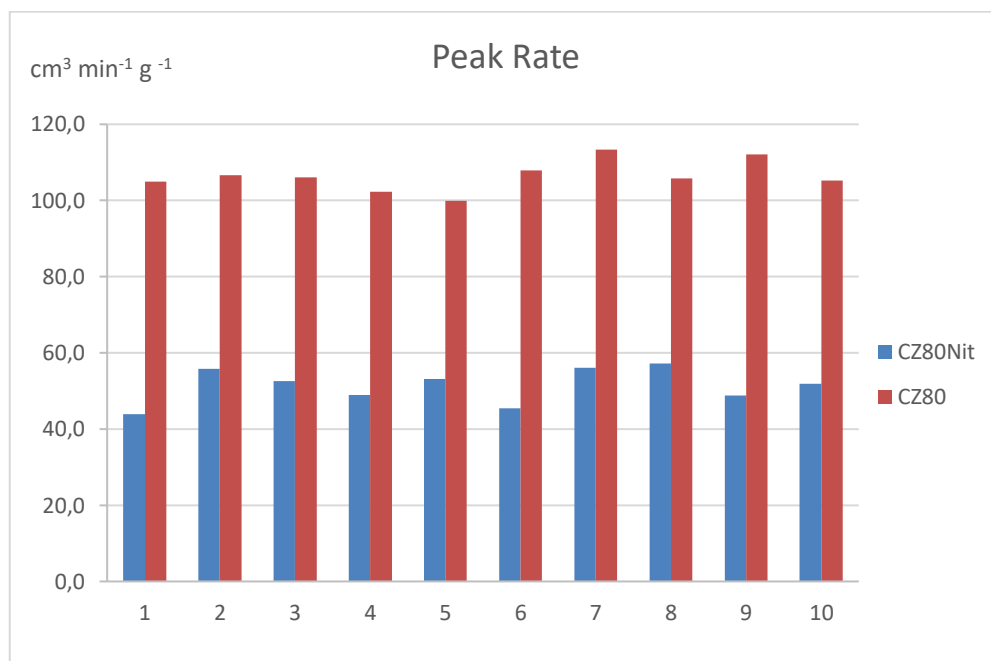


Figure 4.6 Peak rate comparison

| | | | | | | | | | | |
|----------------|----|----|----|----|----|----|----|----|----|----|
| CZ80 | 48 | 52 | 51 | 59 | 53 | 57 | 53 | 54 | 59 | 59 |
| CZ80Nit | 74 | 66 | 84 | 59 | 61 | 74 | 69 | 60 | 74 | 63 |

Table 3 Conversion time, measured in second

4.2.2 Water Splitting results (MS)

We changed measurement device, so we have re-done the hydrogen reduction with the pre-treatment. The set-up of the experiment is the same as described in the paragraph 3.5. As usual the mass of the sample is set to 250 mg.

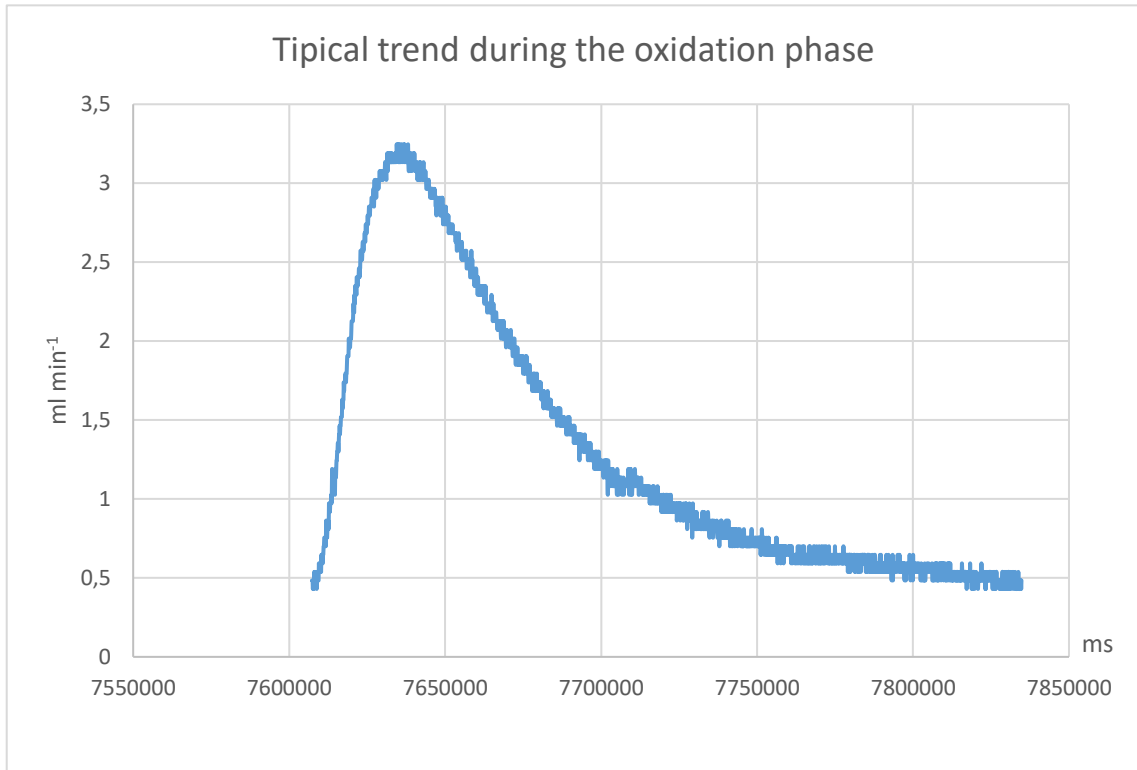


Figure 4.7 Shape of the peak during the oxidation reaction

In the figure the trend of the oxidation phase is presented, the measure is more scattered due to the working principle of the spectrometer.

The conversion time [s]:

| 1 | 2 | 3 | 4 | 5 | 6 | 7 | 8 | 9 | 10 | 11 |
|-----|-----|-----|-----|-----|-----|-----|-----|-----|-----|-----|
| 106 | 222 | 233 | 233 | 210 | 228 | 183 | 177 | 216 | 257 | 213 |

The conversion time is longer respect to the previous one, the cause of this is the reduced flow of the MS test. In fact, in the TCD measurement, the flow is four times greater than in the mass spectrometer measure and the peak is about $60 \text{ cm}^{-3}\text{min}^{-1}\text{g}^{-1}$, instead, the mass spectrometer gives a peak in the order of $15 \text{ cm}^{-3}\text{min}^{-1}\text{g}^{-1}$, while the total hydrogen yield remains equal, this indicates that the peak is flatter.

The hydrogen production and the peak rate are showed in the following figure:

| | <i>HY</i> [$\mu\text{mol g}^{-1}$] | <i>PR</i> [$\text{cm}^3 \text{min}^{-1} \text{g}^{-1}$] |
|----|--------------------------------------|---|
| 1 | 484.9 | 11.9 |
| 2 | 761.0 | 9.2 |
| 3 | 881.1 | 9.8 |
| 4 | 918.7 | 10.2 |
| 5 | 826.1 | 10.8 |
| 6 | 870.5 | 12.3 |
| 7 | 836.4 | 14.1 |
| 8 | 830.9 | 13.2 |
| 9 | 967.7 | 14.2 |
| 10 | 793.0 | 9.1 |
| 11 | 628.6 | 8.0 |

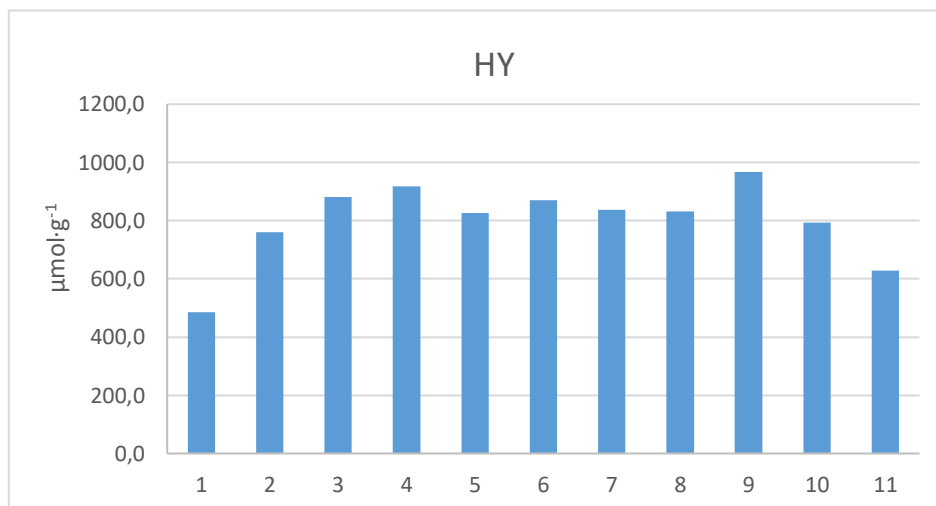


Figure 4.8 Hydrogen yield for each cycle

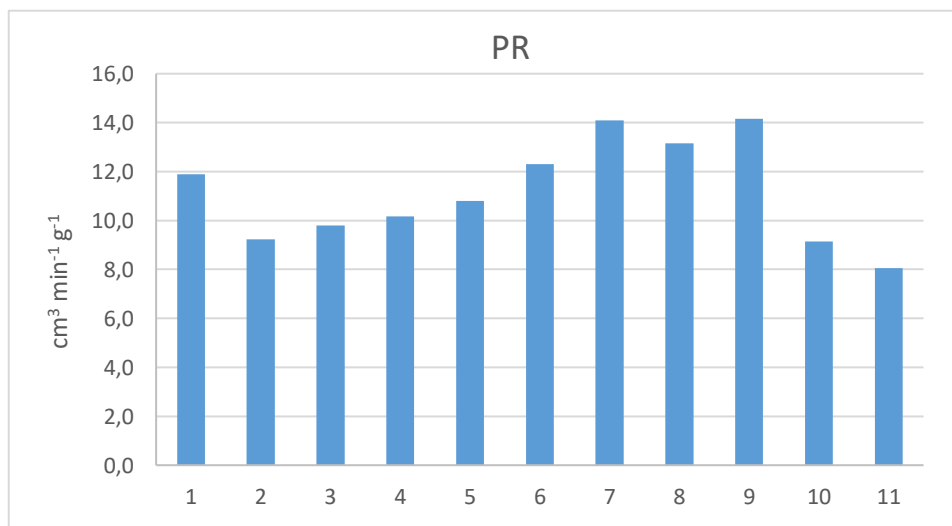
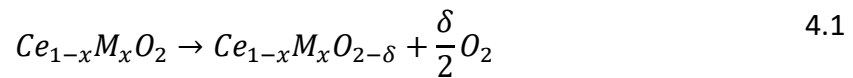


Figure 4.9 Peak rate for each cycle

4.4 CZ80 HSA: WS with thermal reduction

The set of experiment aims to see how the catalysts performs under real water splitting cycle conditions. The water splitting consists in a reduction phase at high temperature, where the metal loses some oxygen ions, then at lower temperature comes the oxidation phase, the reduced metal interacts with the water, capturing the oxygen molecule and releasing hydrogen, the reaction net product. The first phase is an endothermic reaction and needs high temperature, hence high enthalpy, while the oxidation phase is an exothermic reaction. The endothermic reaction requires more energy of that recovered from the exothermic one. The equation for reduction and oxidation phases are the followings:



While in the case of hydrogen reduction the reaction can be assumed as complete, for the thermal reduction it is reported in the literature that the non-stoichiometric reaction occurs (with δ the non-stoichiometric factor) [24], [25].

The oxygen measurement also gives a good indication of the reduction extent, since the more oxygen is freed from the oxide the more water molecules will react with the reduced material, but, in this work we have focused only on the hydrogen production.

4.4.1 The experimental procedure

The experimental procedure differs from the previous hydrogen reduction tests by two main reasons, the first is that we moved towards a complete reaction without the aid of the hydrogen given in the reduction step.. The latter one is that we used another instrument, the mass spectrometer. The start-up cycle consisted in bringing the CZ80HSA, with a ramp of 10°C/min, from room temperature to 1300 °C, followed by a dwelling time of 240 minutes at 1300°C, which is the nitridation treatment, then temperature is reduced to 800, using a ramp of 20°C/min, once to 800°C there is the oxidation, the flow of 120 ml/min becomes a mixture of 90% N₂ and 10% H₂O for 30 minutes.

After the start-up cycle, ten cycles are performed. Each cycle is composed by 4 steps:

- **Ramping:** +10°C/min from 800°C to 1300 °C.
- **Reduction:** in H₂ at 10% and 90% N₂ for 80 minutes.
- **Ramping:** -20 °C/min from 1300°C to 800°C in N₂.
- **Oxidation:** in H₂O at 10% for 30 minutes.

We started to use the mass spectrometer from now on, so we adjusted the flow during the measuring flow to get better data visibility, specifically in the reduction and in the ramping step we used a total flow of 500 ml/min, while in the oxidation, to visually better understand the activity of the sample, we decreased the flow to 120 ml/min.

Unfortunately, this kind of cycle takes 3:30 hours to be completed, which gives room for only two cycles per day.

4.4.2 Results

The results are displayed above. The hydrogen yield, as expected, is lower in comparison to the reduction in hydrogen. The results also show high variability of the yield, with a very low production in the second half of the test cycles.

| | <i>HY [μmol g⁻¹]</i> | <i>PR [cm³ min⁻¹g⁻¹]</i> | <i>toc [s]</i> |
|----|---------------------------------|---|----------------|
| 1 | 156.5 | 4.3 | 88 |
| 2 | 177.7 | 3.6 | 108 |
| 3 | 290.3 | 4.5 | 154 |
| 4 | 4.2 | 1.0 | 6 |
| 5 | 206.5 | 7.8 | 79 |
| 6 | 0.1 | 3.5 | 78 |
| 7 | 0.1 | 1.7 | 23 |
| 8 | 0.1 | 3.0 | 92 |
| 10 | 38.2 | 1.0 | 81 |
| 9 | x | x | x |

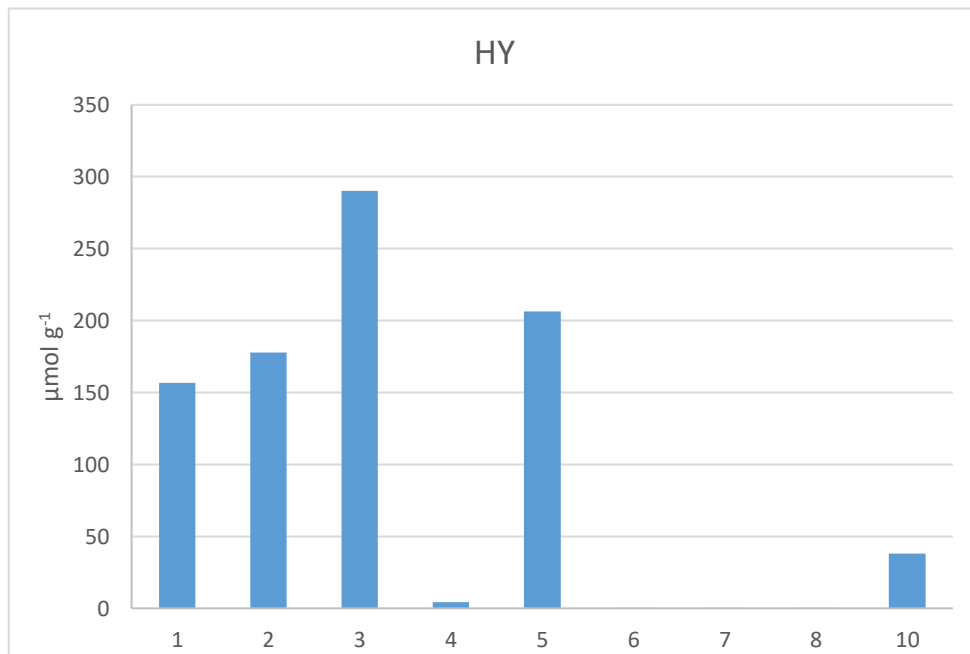


Figure 4.10 Hydrogen yield for each cycle

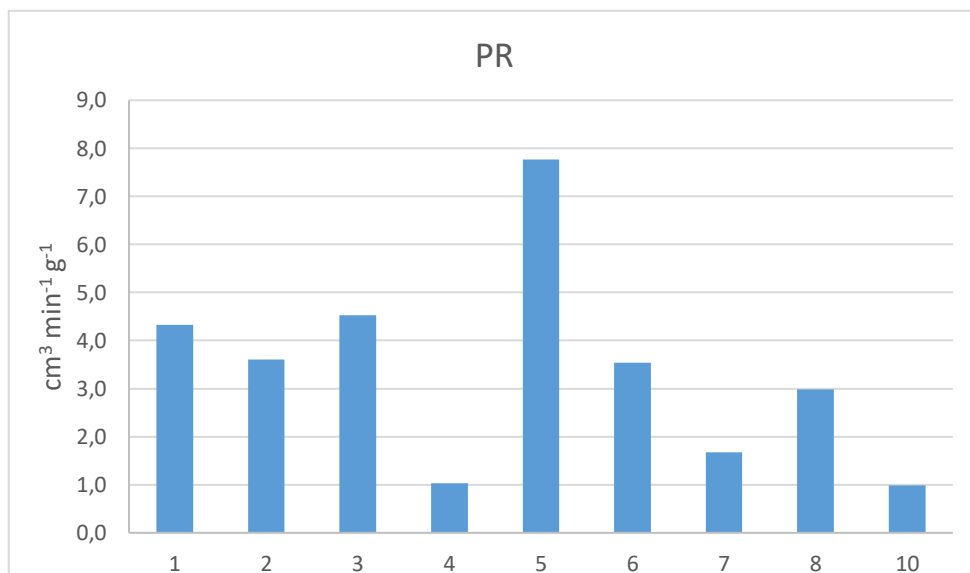


Figure 4.11 Peak for each cycle

As the reader can see the ninth cycle was done with not ideal condition, so it was fail.

4.5 WS on the CZ80 – 0.15SnO₂ with thermal reduction

The sample is one of the twelve synthesized in the chemical department of Udine. The results are better than the previous campaign, but with fluctuating values, meaning that the sample is not stable, leading to scarce reproducibility.

| | <i>HY</i> [$\mu\text{mol g}^{-1}$] | <i>PR</i> [$\text{cm}^{-3} \text{min}^{-1} \text{g}^{-1}$] | <i>toc</i> [s] |
|-----------|--------------------------------------|--|----------------|
| 1 | 457.6 | 16.7 | 117 |
| 2 | 303.7 | 5.3 | 138 |
| 3 | 102.1 | 2.5 | 80 |
| 4 | 433.4 | 15.1 | 116 |
| 5 | 447.1 | 15.4 | 117 |
| 6 | 131.9 | 5.2 | 67 |
| 7 | 289.8 | 11.2 | 76 |
| 8 | 318.2 | 5.8 | 161 |
| 9 | 166.0 | 3.0 | 118 |
| 10 | 300.9 | 5.3 | 129 |

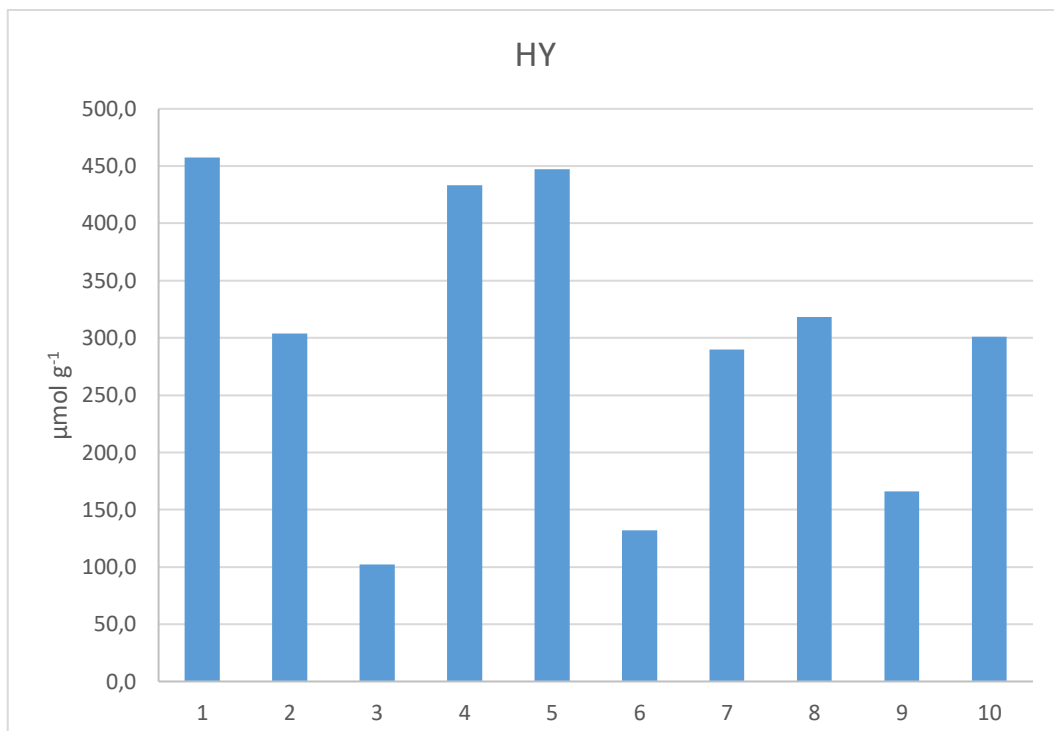


Figure 4.12 Hydrogen yield for each cycle

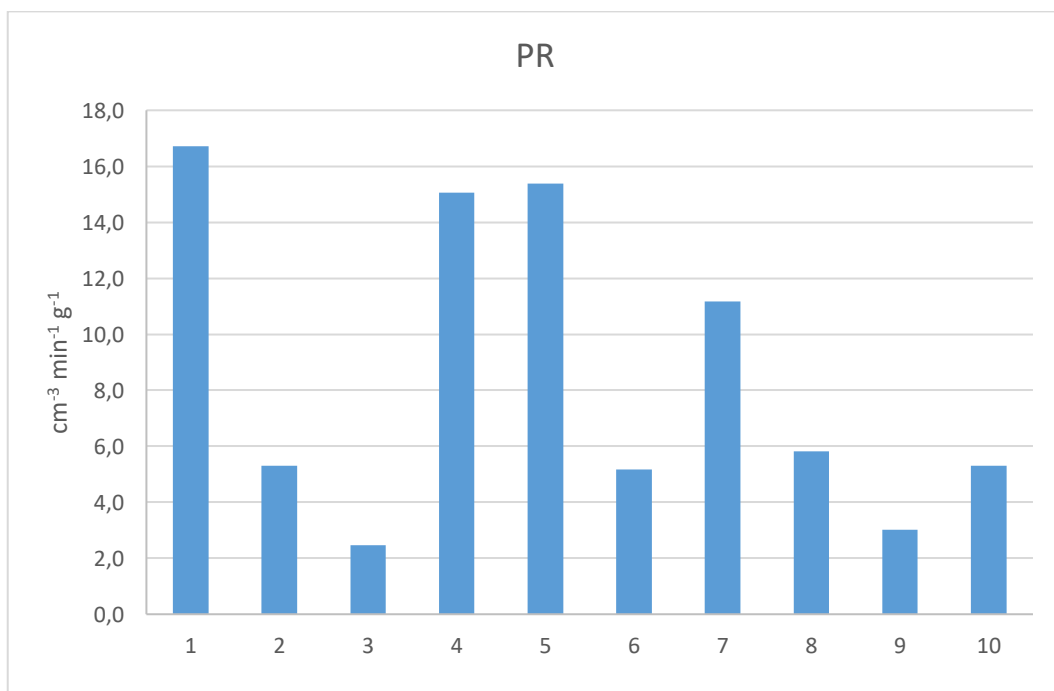


Figure 4.13 Peak rate for each cycle

4.6 WS on CZ20 – 0.25SnO₂ with thermal reduction

The Ceria_{0.2}Zirconia_{0.8} with 25% of Tin oxide was tested for WS splitting with thermal reduction. The test did not show any kind of activity. We also used a different fiberglass that may negative affect the experimental test.

After those tests, we realized that it wasn't worth anymore doing the thermal reduction on the samples, since it took a lot of time and resources to get results that were scarcely reproducible.

For these reasons we turned back to the hydrogen reduction. Unfortunately, even though we tested a fresh CZ20-0.25SnO₂ we didn't get any activity again, meaning that something went wrong during the preparation of the sample or during the thermal treatment. Further discussion about the failed experiments will be done later in this chapter.

4.7 WS on CZ80 – 0.15SnO₂ with hydrogen reduction

Hydrogen reduction was performed at constant 800 °C temperature. Only the thermal treatment was performed at 1300 °C for 4 hours. As usual the mass of the sample was 250 mg. The hydrogen yield is good as the reader can see in the following table, where the conversion time, the hydrogen yield and the peak rate are showed.

| | <i>HY [μmol g⁻¹]</i> | <i>PR [cm³ min⁻¹ g⁻¹]</i> | <i>toc [s]</i> |
|-----------|---------------------------------|--|----------------|
| 1 | 664.5 | 12.1 | 185 |
| 2 | 718.3 | 12.7 | 204 |
| 3 | 777.8 | 12.9 | 211 |
| 4 | 634.0 | 9.8 | 192 |
| 5 | 641.1 | 13.3 | 162 |
| 6 | 570.7 | 9.9 | 171 |
| 7 | 628.9 | 11.7 | 193 |
| 8 | 549.1 | 9.4 | 175 |
| 9 | 473.1 | 9.9 | 160 |
| 10 | 679.8 | 12.1 | 209 |



Figure 4.14 Hydrogen yield for each cycle

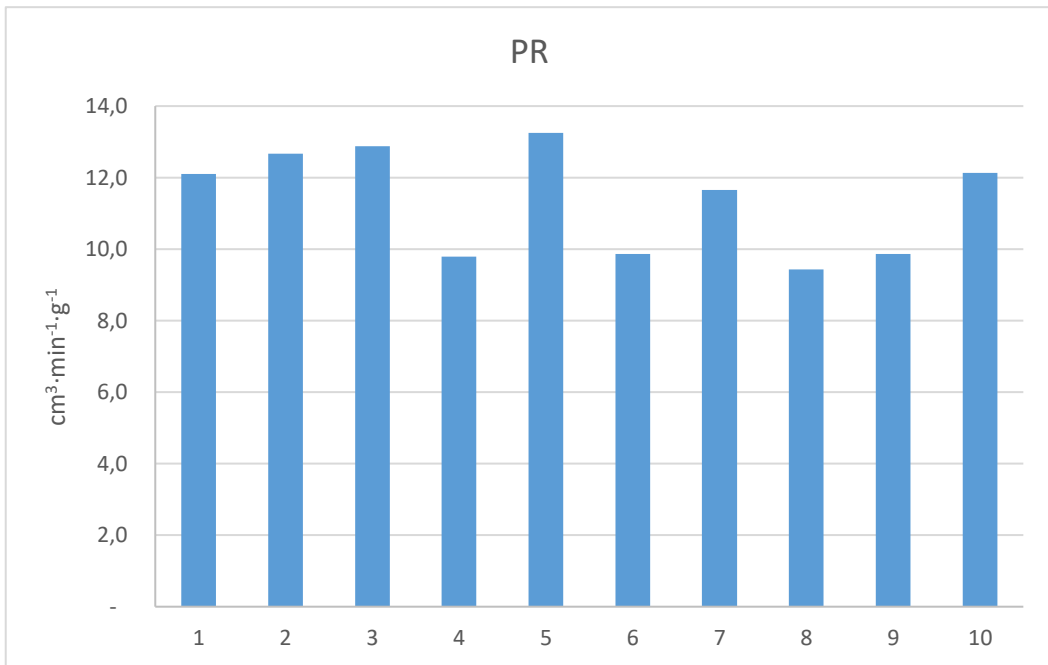


Figure 4.15 Peak rate for each cycle

4.8 WS on CZ20 with hydrogen reduction

A series of tests was performed also on white samples, i.e. the one that do not have percentage of Tin. We only completed this sample due to some internal failure of the furnace that cause the stop of the work.

In the initial part of the test the catalyst worked well, but then, overnight, there was a severe degradation that caused the de-activation of the material, cycle seventh and eighth were particularly affected that they didn't produce the characteristic peak.

| | $[\mu\text{mol g}^{-1}]$ | $[\text{cm}^3 \text{min}^{-1}\text{g}^{-1}]$ | <i>toc [s]</i> |
|----------|--------------------------|--|----------------|
| 1 | 300.2 | 13.8 | 74 |
| 2 | 291.3 | 10.7 | 89 |
| 3 | 204.9 | 7.2 | 88 |
| 4 | 313.1 | 11.2 | 92 |
| 5 | 108.1 | 2.9 | 85 |
| 6 | 72.7 | 2.8 | 52 |
| 7 | 56.0 | 2.4 | 41 |
| 8 | 94.8 | 3.6 | 54 |

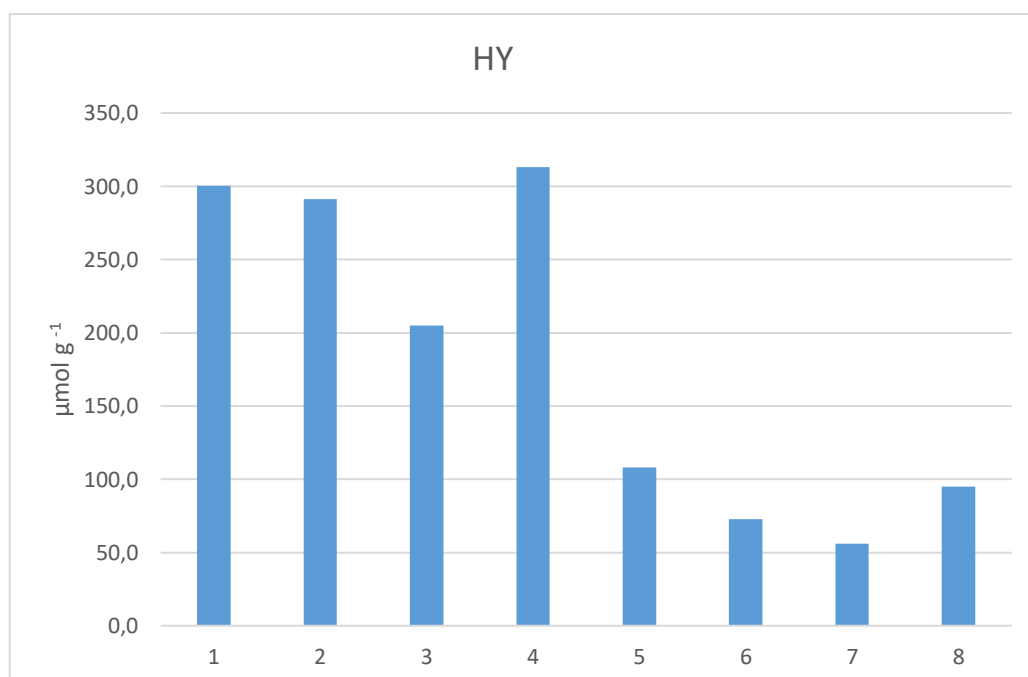


Figure 4.16 Hydrogen yield for each cycle

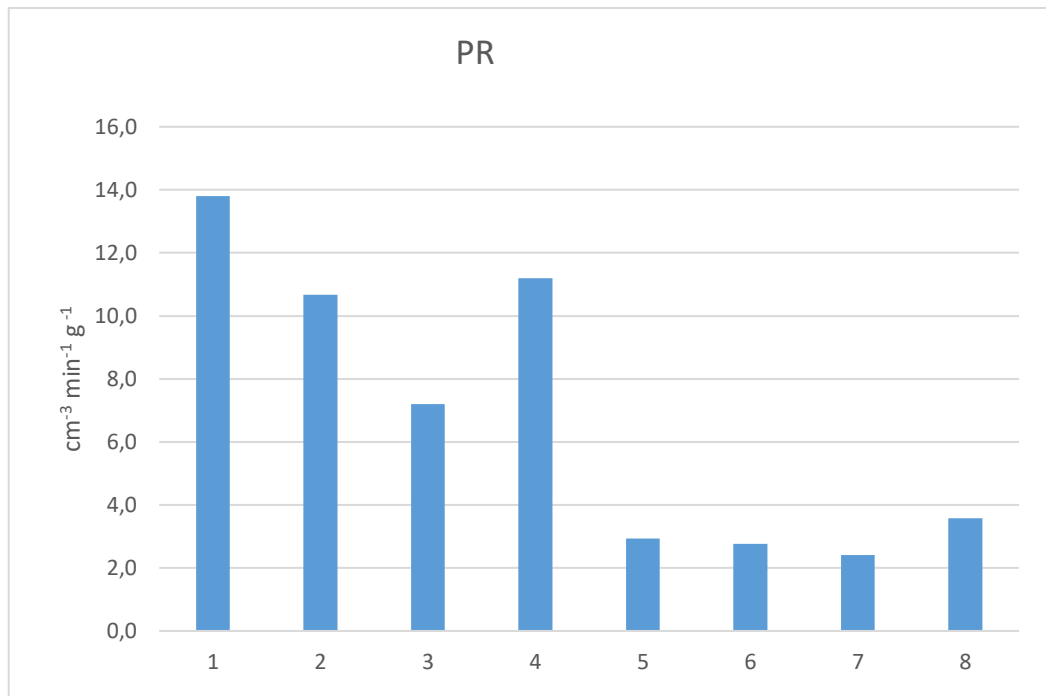


Figure 4.17 Peak rate for each cycle

4.8 WS on CZ50 with hydrogen reduction

The Ceria-Zirconia 50 was tested but already during few cycles we realized that there was no sign of activity, so we stopped. The no activity may be due to the different fiber-glass used to hold the sample in the center of the alumina rod, or the bad synthesis of the sample itself. A *post-mortem* analysis is able to detect if the latter hypothesis is right.

4.9 WS on CZ80 with hydrogen reduction

Lastly, we tested a CZ80 that I synthesized in Udine. The results were underwhelming, we expected a better reduction extent.

| | <i>HY [$\mu\text{mol g}^{-1}$]</i> | <i>PR [$\text{cm}^3 \text{min}^{-1} \text{g}^{-1}$]</i> | <i>toc [s]</i> |
|-----------|--|---|-----------------------|
| 1 | 159.4 | 3.1 | 126 |
| 2 | 201.5 | 4.0 | 140 |
| 3 | 229.4 | 3.2 | 159 |
| 4 | 331.6 | 3.9 | 187 |
| 5 | 240.5 | 3.4 | 153 |
| 6 | 261.9 | 3.5 | 148 |
| 7 | 68.0 | 1.9 | 72 |
| 8 | 215.1 | 2.8 | 173 |
| 9 | 334.8 | 3.2 | 209 |
| 10 | 288.1 | 3.7 | 167 |

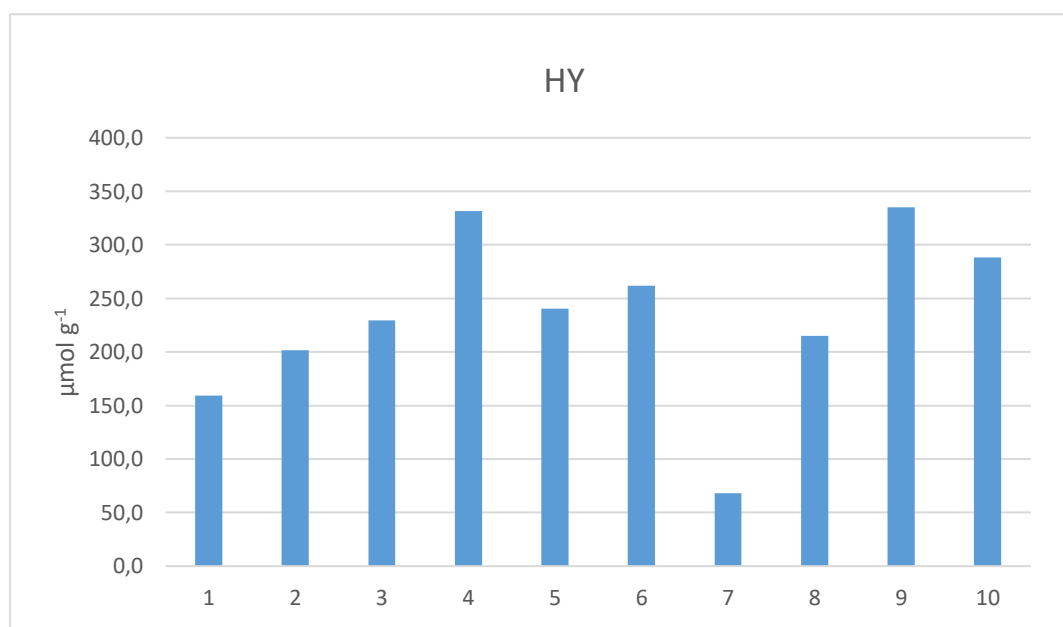


Figure 4.18 Hydrogen yield for each cycle

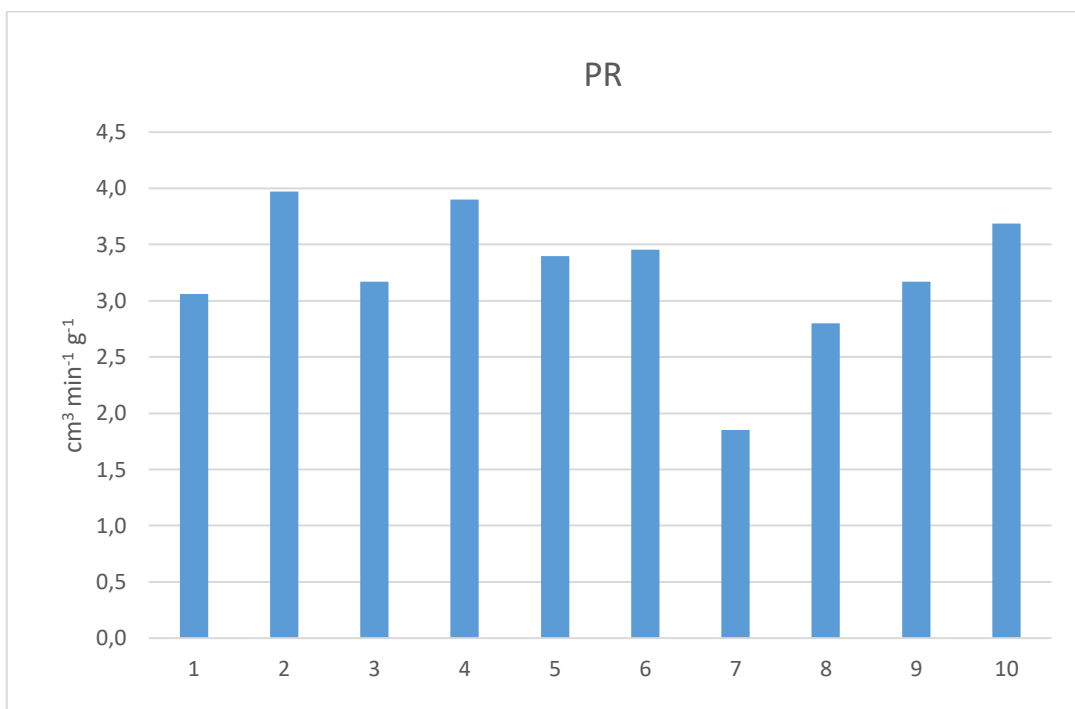


Figure 4.19 Peak rate for each cycle

5 CONCLUSION

The experimental activity was performed using a horizontal furnace operating at ambient pressure, with the aim of testing Ceria-based oxide in water splitting. The sample was placed in a fixed-bed configuration, in a micro-reactor. The experiments are done using two different reduction techniques, hydrogen-assisted reduction and thermal-reduction, both followed with the oxidation reaction, which gives the hydrogen production.

The first four tests on the CZ80 HSA are conducted using the hydrogen-assisted reduction. The difference between the tests are the initial pre-treatment, in air, in pure nitrogen and without pre-treatment. The most productive sample was the one with no pre-treatment, then the nitrogen pre-treatment and, last, the sample aged in air.

The no-thermal treatment scenario is not representative of the real world application, since the thermal reduction reach the temperature of the pre-treatment. This leads to the conclusion that, if the pre-treatment is needed, the best performance is obtained through nitrogen only treatment.

We moved to the thermal reduction of samples before water splitting. The sample tested were the CZ80 HSA, the CZ80-0.15SnO₂ and the CZ20-0.25SnO₂, being the latter two the oxide synthesized in Udine.

Following the previous procedure, the pre-treatment is performed to each sample, then the sample is cycled between thermal reduction (at 1300 °C for 80 minutes) and water splitting. In the thermal reduction cycle the best performance was achieved by the CZ80 Tin doped oxide, although the hydrogen yield and the peak rate did not show constant values through different cycle, hence the cycle showed scarce reproducibility of the test. However, the success of this oxide is the melting of the Tin due to higher operating temperature, as in the liquid phase the oxygen mobility is higher, thus the better performance.

Despite the good results expected from the CZ20 Tin doped oxide, the experiments showed a very bad performance of the material for WS, which both in thermal reduction

and in the hydrogen reduction showed no activity at all, indication that, most probably, was not optimal synthesized [26].

The experiments proceed to the hydrogen reduction of the CZ80-0.15SnO₂, CZ80 and the CZ50. The remarkable findings are that the CZ80 Tin doped sample perform less than the CZ80 HSA, which was not expected, considering the good results in the thermal reduction cycles.

Most probably the oxide decomposition is caused by the thermal-treatment. A *post-mortem* analysis is, in fact, needed in order to verify the causes of the bad performance of some of the oxides, in particular of the CZ20 Tin doped.

In conclusion we find out that, once combined, Zirconia and Tin do not work effectively in synergy together, despite the fact that both are able to enhance the performance of the Ceria when doped.

6 BIBLIOGRAPHY

- [1] BP Energy Outlook 2018 Edition [2] *Solar to fuels conversion technologies: a perspective*, Harry L. Tuller, Renew Sustain Energy (2017).
- [3] Herron, J.A., Kim, J., Upadhye, A.A., Huber, G.W., Maravelias, C.T.: *A general framework for the assessment of solar fuel technologies*. Energy Environ. Sci. 8, 126–157 (2015)
- [4] Kondratenko, E.V., Mul, G., Baltrusaitis, J., Larrazabal, G.O., Perez-Ramirez, J.: *Status and perspectives of CO₂ conversion into fuels and chemicals by catalytic, photocatalytic and electrocatalytic processes*. Energy Environ. Sci. 6, 3112–3135 (2013).
- [5] D. Yadav and R. Banerjee, “A review of solar thermochemical processes” Renew. Sustain. Energy Rev., vol. 54, pp. 497–532, 2016.
- [6] Hinkley JT, Mcnaughton RK, Neumann A. *Development of a high flux solar furnace facility at CSIRO for Australian Research and Industry*. In: Proceedings of the 48th AuSES Annual Conference on Solar 2010, Canberra, ACT, Australia; 2010. p.1–9.
- [7] C. Agrafiotis, M. Roeb, and C. Sattler, “A review on solar thermal syngas production via redox pair-based water/carbon dioxide splitting thermochemical cycles” Renew. Sustain. Energy Rev., vol. 42, pp. 254–285, 2015.
- [8] Scheffe JR, LiJ, Weimer AW. *A spinel ferrite/hercynite water-splitting redox cycle*. Int J Hydrogen Energy 2010; 35:3333–40.
- [9] Chongyan Ruan , Yuan Tan, “A Novel CeO₂-xSnO₂/Ce₂Sn₂O₇ Pyrochlore Cycle for Enhanced Solar Thermochemical Water Splitting”, American Institute of Chemical Engineers AIChE J, 63: 3450–3462, 2017

- [10] C.J. Brinker, G.W. Scherer, 1990. *Sol-gel Science. The Physics and Chemistry of Sol-Gel Processing*. Academic Press Inc..
- [11] M.P. Pechini, U.S. Patent 3,330,697, 1967.
- [12] Beom-Kyeong Park, Jong-Won Lee, Seung-Bok Lee, Tak-Hyoung Lim, Seok-Joo Park, Rak-Hyun Song, Won Bin Im, Dong-Ryul Shin, *La-doped SrTiO₃ interconnect materials for anode-supported flat-tubular solid oxide fuel cells*, International Journal of Hydrogen Energy, Volume 37, Issue 5, 2012, Pages 4319-4327, ISSN 0360-3199
- [13] [https://www.artisantg.com/Scientific/74393/TA_Instruments_SDT_Q600 Simultaneous_TGA_DSC](https://www.artisantg.com/Scientific/74393/TA_Instruments_SDT_Q600_Simultaneous_TGA_DSC)
- [14] Brunauer et al. 1938, ISO 9277:2010, DIN ISO 9277:2013
- [15] http://www.micromeritics.com/Repository/Files/TriStar_3000_Operators_Manual_V6.08.pdf
- [16] <https://www.malvernpanalytical.com/en/products/product-range/xpert3-range/xpert3-powder/index.html>
- [17] <http://www.lentonfurnaces.com/content42/LTF-Tube-furnaces-1400C-1500C-1600C.aspx>
- [18] <https://analyzedetectnetwork.com/manual.php?m=VErDsstxWhtn>
- [19] Grob, Robert L. Ed.; "Modern Practice of Gas Chromatography", John Wiley & Sons, C1977, pg. 228
- [20] http://www.uniroma2.it/didattica/MA2/deposito/spettrometria_massa.pdf
- [21] <http://www.spectroscopyonline.com/detecting-ions-mass-spectrometers-faraday-cup>
- [22] A.Pica, "Experimental analysis of materials for CO₂ reduction via chemical looping", 2017.
- [23] <http://www.massspecpro.com/detectors/electron-multiplier>

- [24] Panlener, R.J., Blumenthal, R.N., & Garnier, J.E. (1975). "A thermodynamic study of nonstoichiometric cerium dioxide." *Journal of Physics and Chemistry of Solids*, 36(11), 1213-1222.
- [25] Bulfin, B., et al. "Statistical thermodynamics of non-stoichiometric ceria and ceria zirconia solid solutions." *Physical Chemistry Chemical Physics* 18.33 (2016): 23147-23154.
- [26] Dong, Qiang, et al. "Hydrothermal synthesis of tin doped ceria-zirconia solid solutions with enhanced thermal stability and oxygen storage capacity." *RSC Advances* 2.33 (2012): 12770-12774.